

## 6. Rheology of hyperbranched polymer melts

### 6.1. Introduction

The rheological properties of hyperbranched polymer fluids under shear flow, such as the shear viscosity and first and second normal stress coefficients, can be calculated from the components of the molecular pressure tensor (Todd and Daivis, 2007) given by:

$$\mathbf{P}^M V = \left\langle \sum_{i=1}^N \frac{\mathbf{p}_i \mathbf{p}_i}{M_i} - \frac{1}{2} \sum_{i=1}^N \sum_{\alpha=1}^{N_s} \sum_{j \neq i}^N \sum_{\beta=1}^{N_s} \mathbf{r}_{ij} \mathbf{F}_{i\alpha j\beta} \right\rangle \quad (6.1)$$

where  $\mathbf{p}_i$  represents the total peculiar centre of mass momentum of molecule  $i$ , as defined by the equations of motion,  $\mathbf{r}_{ij} = \mathbf{r}_j - \mathbf{r}_i$  is the centre of mass separation of molecule  $i$  and  $j$ ,  $\mathbf{F}_{i\alpha j\beta}$  is the intermolecular force on bead  $\alpha$  in molecule  $i$  due to bead  $\beta$  in molecule  $j$  and  $N_s$  is the total number of interacting beads in a molecule. The angular brackets denote an average over the non-equilibrium steady state.

The time average of the molecular pressure tensor is symmetric and equal to the time average of the atomic pressure tensor which is given by:

$$\mathbf{P}^A V = \left\langle \sum_{i=1}^N \sum_{\alpha=1}^{N_s} \frac{\mathbf{p}_{i\alpha} \mathbf{p}_{i\alpha}}{m_{i\alpha}} - \frac{1}{2} \sum_{i=1}^N \sum_{\alpha=1}^{N_s} \sum_{j \neq i}^N \sum_{\beta=1}^{N_s} \mathbf{r}_{i\alpha j\beta} \mathbf{F}_{i\alpha j\beta} - \sum_{i=1}^N \sum_{\alpha=1}^{N_s-1} \sum_{\beta > \alpha}^{N_s} \mathbf{r}_{i\alpha j\beta} \mathbf{F}_{i\alpha j\beta} \right\rangle \quad (6.2)$$

where  $\mathbf{r}_{i\alpha j\beta}$  is the separation between bead  $\alpha$  in molecule  $i$  and bead  $\beta$  in molecule  $j$  and  $\mathbf{p}_{i\alpha}$  represents the atomic momentum. In this work, only the molecular pressure tensor has been calculated.

The non-Newtonian shear viscosity of hyperbranched polymer fluids subject to planar shear flow, where the fluid flows in the  $x$  direction with velocity gradient in the  $y$  direction, can be calculated from the components  $P_{xy}$  and  $P_{yx}$  of the molecular pressure tensor  $\mathbf{P}^M$  as:

$$\eta = -\left( \langle P_{xy} \rangle + \langle P_{yx} \rangle \right) / 2\dot{\gamma}. \quad (6.3)$$

The first and second normal stress coefficients can be computed as:

$$\psi_1 = \frac{\langle P_{yy}^M \rangle - \langle P_{xx}^M \rangle}{\dot{\gamma}^2} \quad (6.4)$$

$$\psi_2 = \frac{\langle P_{zz}^M \rangle - \langle P_{yy}^M \rangle}{\dot{\gamma}^2} \quad (6.5)$$

whereas the isotropic hydrodynamic pressure of the system is obtained from:

$$p = \frac{1}{3} \text{Tr}(\mathbf{P}_M) = \frac{1}{3} (\langle P_{xx}^M \rangle + \langle P_{yy}^M \rangle + \langle P_{zz}^M \rangle) \quad (6.6)$$

## 6.2. Shear viscosity

### 6.2.1. Shear viscosity for hyperbranched polymers of different molecular weights

The viscosities at various shear rates computed for type A hyperbranched polymers of different molecular weights using *NVT* simulations are presented in Figure 6.1. As can be seen, at the same strain rate, larger hyperbranched polymers always have higher viscosity values. It can also be seen that the range of strain rates considered is large enough to capture the shear thinning behaviour of all simulated hyperbranched polymer systems. At low strain rates, the viscosities remain constant whereas at high strain rates, these values decrease rapidly. This property of polymeric fluids is very important for many engineering applications.

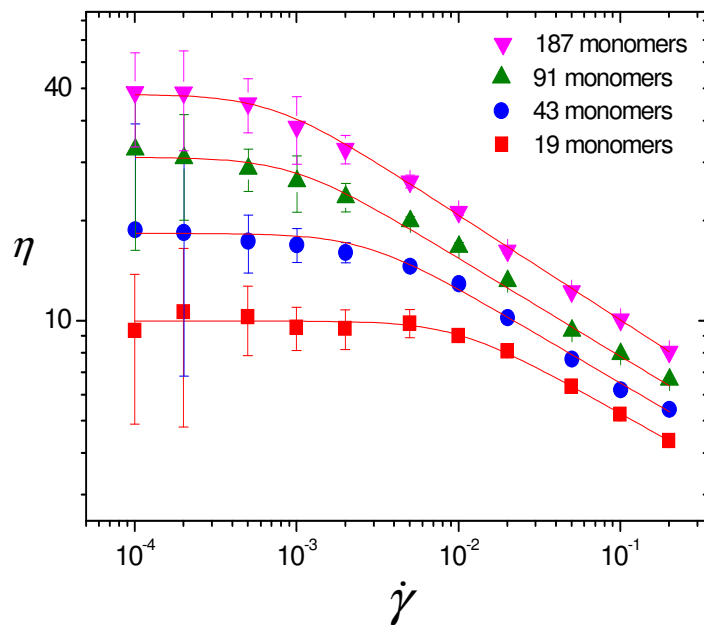


**Figure 6.1.** Dependence of shear viscosity on strain rate for type A hyperbranched polymers of different molecular weights (solid lines representing fitting with the Carreau-Yasuda model).

Shear viscosity data for different hyperbranched polymers in Figure 6.1 were fitted using the Carreau-Yasuda model (Bird et al., 1987) which is given by:

$$\eta = \eta_0 / \left[ 1 + (\lambda_\eta \dot{\gamma})^2 \right]^{p_\eta} \quad (6.7)$$

where  $\eta_0$  is the zero shear viscosity,  $\lambda$  is a time constant and  $p$  is the power law exponent. The fitting parameters obtained for simulated type A hyperbranched polymers of different molecular weights are presented in Table 6.1.

**Table 6.1. Parameters of the Carreau-Yasuda model fitted to the shear viscosity versus strain rate dependence of type A hyperbranched polymers.**

Number of beads	$\eta_0$	$\lambda_\eta$	$p_\eta$
19	10(2)	101(8)	0.138(1)
43	18(3)	378(237)	0.143(5)
91	31(11)	1069(299)	0.148(8)
187	48(6)	1422(615)	0.158(2)

Apart from using the Carreau-Yasuda model, an alternative way to obtain the zero shear rate viscosity is by using the Cross equation (Cross, 1965), given as:

$$\eta = \eta_\infty + (\eta_0 - \eta_\infty) / (1 + (K \dot{\gamma})^{m_c}) \quad (6.8)$$

where  $\eta_\infty$  is the infinite shear viscosity,  $K$  is the consistency index and  $m_c$  is the power law index. The disadvantage of the Cross model is that in experiment, it is difficult to measure the infinite shear rate viscosity  $\eta_\infty$ , therefore it is often set to be a very small value (Yasuda, 2006). Cross equation fitting parameters for shear viscosity data are shown in Table 6.2. The zero shear viscosities for hyperbranched polymers composed of 19, 43 and 91 beads obtained from Cross equation fitting are quite similar to those from the Carreau-Yasuda model.

**Table 6.2. Parameters of the Cross equation fitted to the shear viscosity versus strain rate dependence for type A hyperbranched polymers.**

Number of beads	$\eta_0$	$\eta_\infty$	$K$	$m_c$
19	10 (2)	4(1)	24(9)	1.3(4)
43	18.6(3)	3.2(9)	60(10)	0.78(9)
91	35(1)	2(1)	178(20)	0.56(5)
187	53(2)	6(1)	310(41)	0.71(8)

Figure 6.2 presents the fitted lines obtained from the Cross equation in comparison with the Carreau-Yasuda equation for shear viscosity data of type A hyperbranched polymer comprising 187 monomers. It can be seen that these two models agree very well. Fitted lines are slightly different at very high shear rates, in the transition region from Newtonian to non-Newtonian and at very low shear rates.

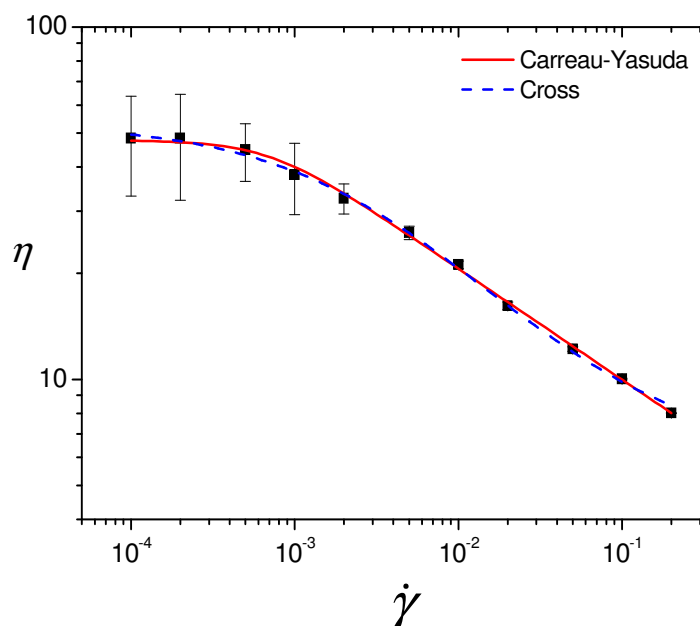
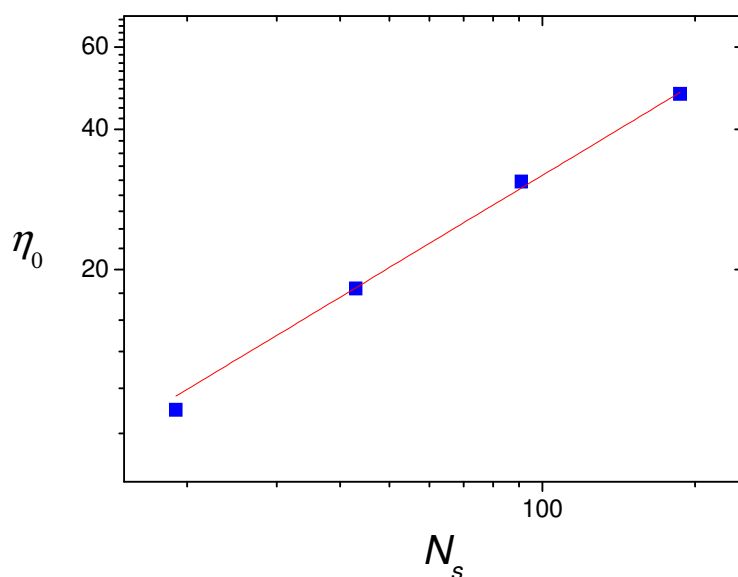
**Figure 6.2. Carreau-Yasuda equation vs. Cross equation fitted for shear viscosity data for type A hyperbranched polymers composed of 187 monomers.**

Figure 6.3 presents the dependence of the zero shear rate viscosity on the number of beads per molecule for different hyperbranched polymers. The zero shear rate viscosity scales as  $\eta_0 \propto N_s^{0.657(2)}$  where  $N_s$  is the number of monomers/beads per molecule. The exponent of

the power law for hyperbranched polymer melts is consistent with that for dendrimers which were found to have  $\eta_0 \propto N_s^{0.646(2)}$  (Bosko et al., 2004b) due to similar molecular structures. Furthermore, our results suggest that hyperbranched polymers are free of entanglements as the dependence of viscosities on the number of monomers does not break into two regions at low and high number of monomers, whereas most of the linear analogues have viscosity dependencies given as  $\eta_0 \propto M_w$  at low molecular weights and  $\eta_0 \propto N_s^{3.4}$  at high molecular weights where the polymer chains entangle (Doi and Edwards, 1986). However as WCA and FENE potentials were employed to simulate hyperbranched polymers, beads along the polymer chain can vibrate and rotate freely. This results in a polymer model that is more flexible than typical real materials and model molecules in shearing dense fluids may fold upon themselves more than in reality. It has been found experimentally that the value of the power law exponent for dendrimers is approximately 1.1 (Hawker et al., 1995, Farrington et al., 1998, Uppuluri et al., 2000) which is quite high compared to that from NEMD simulations which was found to be 0.646(2). Therefore higher shear viscosity and higher values of the power law exponent are expected in experiments on common hyperbranched polymers.



**Figure 6.3. Zero shear viscosity vs. number of beads per molecule for hyperbranched polymers of type A.**

The time constant  $\lambda$  in the Carreau-Yasuda model fitted to the simulation data is also the longest relaxation time of molecules composing the fluids. Although the longest relaxation

time  $\tau_0$  can be the rotational relaxation time or the reptation relaxation time,  $\tau_0$  can be considered to be the rotational relaxation time as there is no entanglement in these hyperbranched polymer systems and hence there is no reptation relaxation time. On the other hand, the inverse of the time constant  $\lambda$  is the strain rate  $\dot{\gamma}_0$  at which the onset of shear thinning is observed. For type A hyperbranched polymers with 19, 43, 91 and 187 beads, the values of  $\dot{\gamma}_c$  are  $9.9(5)\times 10^{-3}$ ,  $2.6(4)\times 10^{-3}$ ,  $9.35(3)\times 10^{-4}$  and  $7.032(2)\times 10^{-4}$  respectively. The shear thinning behaviour occurs at lower strain rates for large hyperbranched molecules in comparison with small hyperbranched polymers. This can be explained by relaxation times, the deformation and tendencies to align with the shear flow. Shear thinning occurs due to the deformation and increased alignment of the molecules to the flow field, which is directly related to the relaxation time  $\tau_0$  (Kioupis and Maginn, 1999). At shear rates higher than the inverse of  $\tau_0$ , molecules are stressed and in order to reduce the stress, the molecules extend, deformation occurs and alignment increases, the fluid moves into the non-Newtonian regime and the new structural configuration results in lower viscosity. Because larger molecules have longer relaxation time  $\tau_0$ , the value of  $1/\tau_0$  is smaller than that of small molecules and the fluids composed of large polymers exhibit the crossover from Newtonian to non-Newtonian behaviour at lower strain rates. The stretching caused by the applied shear results in a more asymmetric ellipsoidal configuration of hyperbranched polymers which has been discussed in detail in the previous Chapter.

Figure 6.4 presents the dependence of longest relaxation times  $\tau_0$  on the number of beads per molecule  $N_s$  for four type A hyperbranched polymer systems. The logarithm of  $\tau_0$  for hyperbranched polymers composed of 19, 43 and 91 beads has a linear relationship with the logarithm of the number of beads  $N_s$ . The relaxation time for these systems scales as  $\tau_0 \propto N_s^{1.4(2)}$ . The exponent value of 1.4(2) for hyperbranched polymers is consistent with previous NEMD simulation results which found that the exponent value is 1.7 for linear polymers and 1.3 for dendrimers (Bosko, 2005). Our exponent result is lower than those predicted by the Rouse model which gives  $\tau_0 \propto M^2$  (Doi and Edwards, 1986). On the other hand the value of  $\tau_0$  for the largest hyperbranched polymer system comprising 187 beads does not follow the same trend of

the smaller polymers. The main causes might be the increase of structural rigidity with the number of beads  $N_s$  and the flow-induced stretching behaviour of hyperbranched polymers which results in the more aspherical shape of small molecules and more spherical shape of large molecules. This is opposite to the behaviour of linear molecules. For long linear polymers above the critical value of  $N_s$ , the longest relaxation time, which is predicted to scale as  $N_s^3$  by the reptation theory, results from the entanglement of long chains (Doi and Edwards, 1986). This is less likely to be the case for hyperbranched polymers with short branches and a large number of terminal groups. Furthermore our computed values of the longest relaxation time have large uncertainties due to the multi-step procedure used to obtain them.

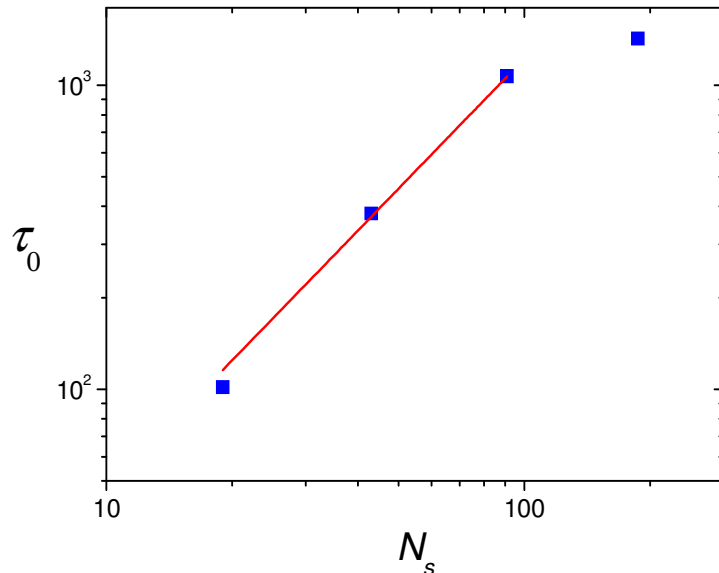


**Figure 6.4.** Longest relaxation time versus number of beads per molecule for type A hyperbranched polymers.

The Weissenberg number  $Wi$  is a dimensionless number that can be calculated from the longest relaxation time by the definition  $Wi = \dot{\gamma}\tau_0$ . Unlike the Deborah number which is used to describe flows with a non-constant stretch history, the Weissenberg number describes the flow with a constant stretch history. Figure 6.5 presents the dependence of the ratio of shear viscosity and zero shear rate viscosity on the Weissenberg number for different hyperbranched polymers. It can be seen that the ratios of shear viscosity to zero shear rate viscosity obtained from NEMD simulations for four hyperbranched polymer systems show a significant degree of consistency with a single master curve.

At  $Wi \approx 1$ , the value of  $\eta/\eta_0$  for all polymers starts to decrease. The computed data were fitted with the Carreau-Yasuda model and give a dependence of  $\eta/\eta_0$  on the Weissenberg number as  $\eta/\eta_0 = 0.996(9)/[1 + (1.1(1) \times Wi)^2]^{0.143(6)}$ . Using the master curve established, the shear rate dependence of the viscosity of other hyperbranched polymers in this series could be predicted.

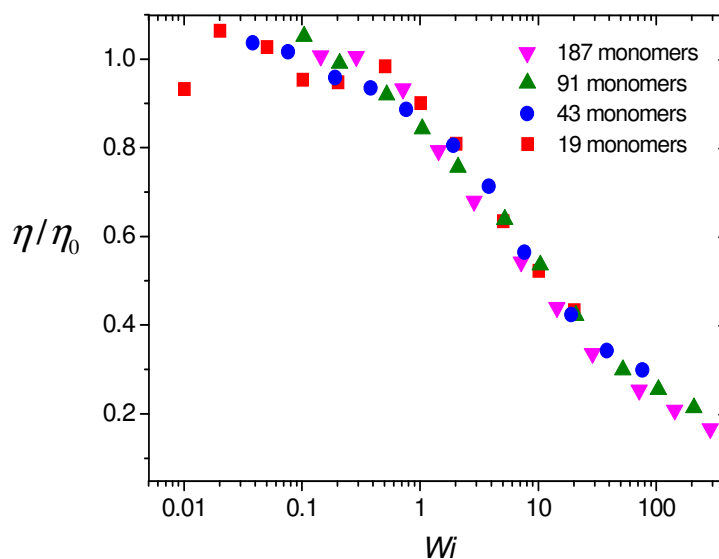


**Figure 6.5. Dependence of the ratio  $\eta/\eta_0$  on the Weissenberg number for type A hyperbranched polymers of different molecular weights.**

### *6.2.2. Shear viscosities for hyperbranched polymers with different numbers of spacers*

Shear viscosity data at different strain rates obtained from  $NpT$  and  $NVT$  simulations for hyperbranched polymers with the same molecular weight of 187 beads but different numbers of spacers are presented in Figure 6.6. As can be seen, the shear thinning behaviour is captured within the considered range of strain rates for hyperbranched polymers of all types. The viscosities reach a plateau at low strain rates then decrease rapidly at high strain rates. Furthermore, the viscosities of simulated fluids increase with increasing number of spacers. Hyperbranched polymers of type A possess the lowest shear viscosities whereas polymers of type D have the highest viscosities. This is because hyperbranched polymers with a larger number of spacer units have longer branches and more open structure, which can lead to more entanglement in the systems and result in higher values of viscosity.

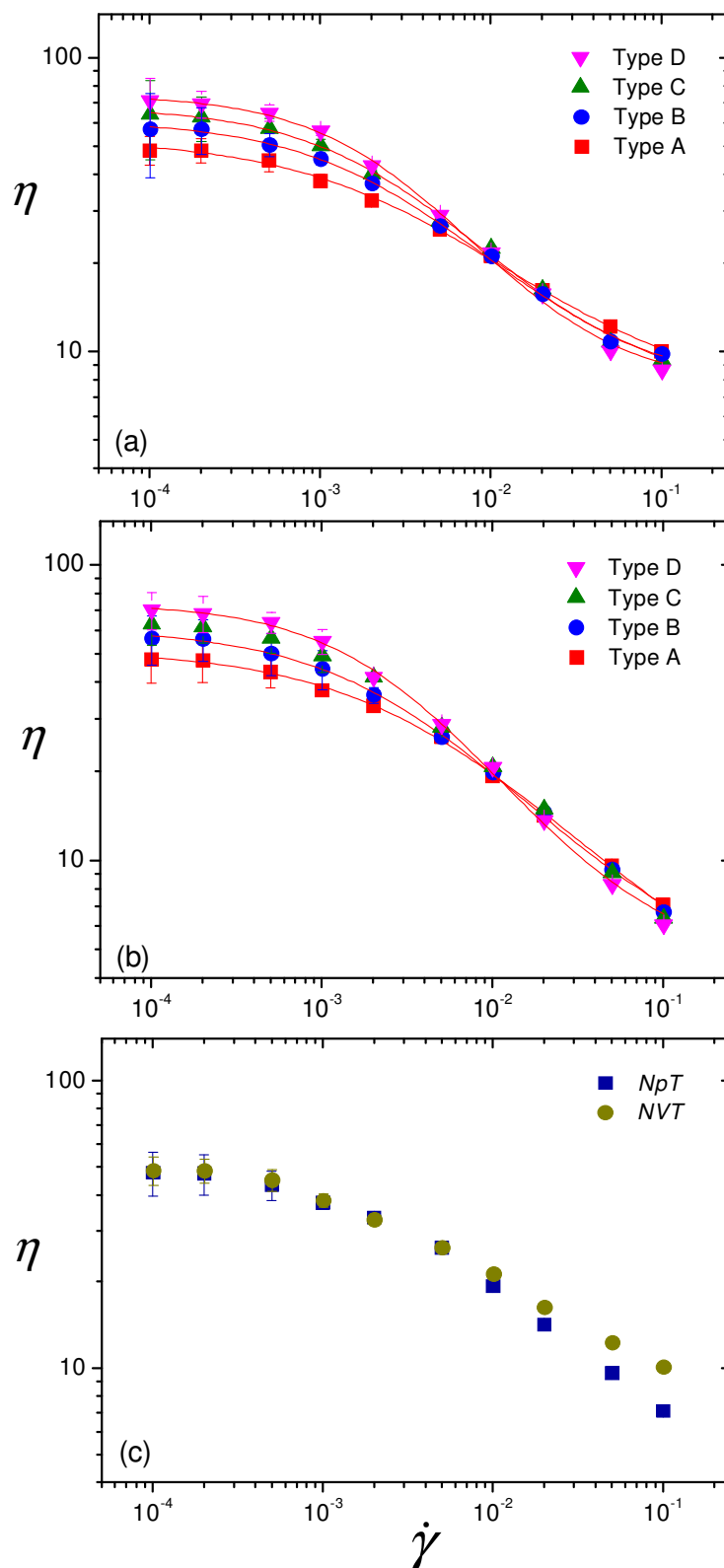


Figure 6.6. Shear viscosities versus strain rate for 187 bead hyperbranched polymers (a) of different types in *NVT* simulations, (b) of different types in *NpT* simulations and (c) of type A in *NVT* and *NpT* simulations (solid lines representing fitting with the Cross model).

Results obtained from  $NVT$  and  $NpT$  simulations only differ from each other at high strain rates as they apply to different state points. Viscosities in the high strain rate region obtained from constant pressure simulations are lower than those from constant volume simulations. The reason for the more pronounced shear thinning behaviour in  $NpT$  simulations is because of the ‘shear dilatancy’ – the density decreases as the shear rate increases. However  $NpT$  and  $NVT$  simulation results will be the same if the same state point is investigated by setting the required pressure in  $NpT$  simulations equal to the pressure obtained from  $NVT$  simulations at a given strain rate (Daivis and Evans, 1994).

Viscosity data for these polymers were fitted using the Cross equation, as given in Eq. 6.8. Fitting parameters are shown in Table 6.3. The  $NpT$  simulation zero shear rate viscosities obtained from the Cross equation fit are then plotted against the number of spacers and results are shown in Figure 6.7. It can be clearly seen that zero shear rate viscosities correlate linearly with the number of spacers  $b$  in the hyperbranched polymer systems simulated. The slope of the linear fit is found to be 7.3(2). The linear dependence of  $\eta_0$  on number of spacers has also been found in Brownian dynamics simulations (Lee and McHugh, 2001) for hyperbranched polymers comprising 66 beads per molecule and in experiments (Markoski et al., 2001) for hyperbranched aromatic etherimide copolymers.

**Table 6.3. Parameters of the Cross model fitted to the shear viscosity versus strain rate dependence for 187 bead hyperbranched polymers with different numbers of spacers.**

Type of hyperbranched polymers	$NVT$				$NpT$			
	$\eta_\infty$	$\eta_0$	$K$	$m_C$	$\eta_\infty$	$\eta_0$	$K$	$m_C$
A	7(2)	53(2)	322(46)	0.74(9)	3(2)	52(1)	241(24)	0.72(7)
B	7(1)	61(1)	374(28)	0.86(6)	4(1)	60(1)	336(25)	0.81(6)
C	7(1)	67(1)	391(30)	0.90(7)	3(1)	67(1)	347(21)	0.82(5)
D	8(2)	74(2)	408(30)	1.01(8)	5(1)	74(2)	380(30)	0.96(8)

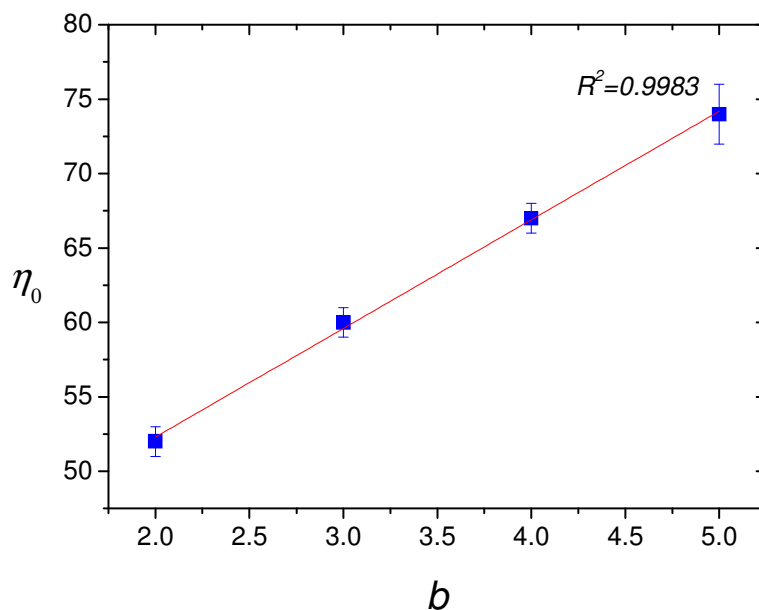


**Figure 6.7. Dependence of zero shear rate viscosities on the number of spacers for 187 bead hyperbranched polymers.**

Viscosity data were also fitted using Carreau-Yasuda equation, given by  $\eta = \eta_0 / \left[ 1 + (\lambda_\eta \dot{\gamma})^2 \right]^{p_\eta}$ . The fitting parameters for all simulated hyperbranched polymer systems are presented in Table 6.4. The inverse of the time constant  $\lambda_\eta$  is the critical strain rate  $\dot{\gamma}_c$  at which the onset of shear thinning is observed. As the values of  $\lambda_\eta$  increase with increasing number of spacers, the critical strain rate  $\dot{\gamma}_c$  is lowest for hyperbranched polymers of type A with the lowest Wiener index and highest for polymers of type D with the largest Wiener index. A similar behaviour of the critical strain rate was found for hyperbranched polymers under elongational flow in Brownian simulations (Neelov and Adolf, 2004). Furthermore the time constants in the Carreau-Yasuda model fitted to the shear viscosity data from  $NpT$  simulations are always lower than those from  $NVT$  simulations. Therefore the value of the critical strain rate for a given hyperbranched polymer system at constant pressure is always higher than that at constant volume. The advantage of  $NpT$  simulations over  $NVT$  simulations is that  $NpT$  data are more comparable to experiments. However, as mentioned above,  $NVT$  and  $NpT$  algorithms will give the same results if the same state point is investigated.

**Table 6.4. Parameters of the Carreau-Yasuda model fitted to the shear viscosity versus strain rate dependence for 187 bead hyperbranched polymers with different numbers of spacers.**

Type of hyperbranched polymers	$NVT$			$NpT$		
	$\eta_0$	$\lambda_\eta$	$p_\eta$	$\eta_0$	$\lambda_\eta$	$p_\eta$
A	48(6)	1422(615)	0.158(2)	47(1)	1338(240)	0.18(1)
B	57.5(4)	1524(87)	0.186(4)	56.0(7)	1471(137)	0.200(8)
C	63(5)	1612(93)	0.195(5)	62.2(7)	1562(127)	0.214(8)
D	75(19)	1918(1268)	0.214(9)	69.6(5)	1801(730)	0.245(7)

The time constant  $\lambda_\eta$  in the Carreau-Yasuda model fitted to the viscosity data is also the longest relaxation time  $\tau_0$  of molecules composing the fluids, from which the Weissenberg number  $Wi$  can be calculated by the definition  $Wi = \dot{\gamma}\tau_0$ . As shown in the previous section, using the Weissenberg number, a master curve can be established and the shear rate dependence of the viscosity for hyperbranched polymers of different molecular weights in the same series could be predicted. With the same purpose, the ratios of shear viscosity and zero shear rate viscosity for hyperbranched polymers of four different architectures are plotted against the Weissenberg number and results are shown in Figure 6.8. However results show that using the Weissenberg number calculated from the time constant in the Carreau-Yasuda model and normalized viscosity is not sufficient to eliminate the differences between different architectures. Therefore the time constant in the Cross model is used to compute the Weissenberg number and viscosity data were normalized using different parameters in the Cross models. Although this gives a better result in eliminating the differences between simulated architectures, a master curve still cannot be established, as shown in Figure 6.9.

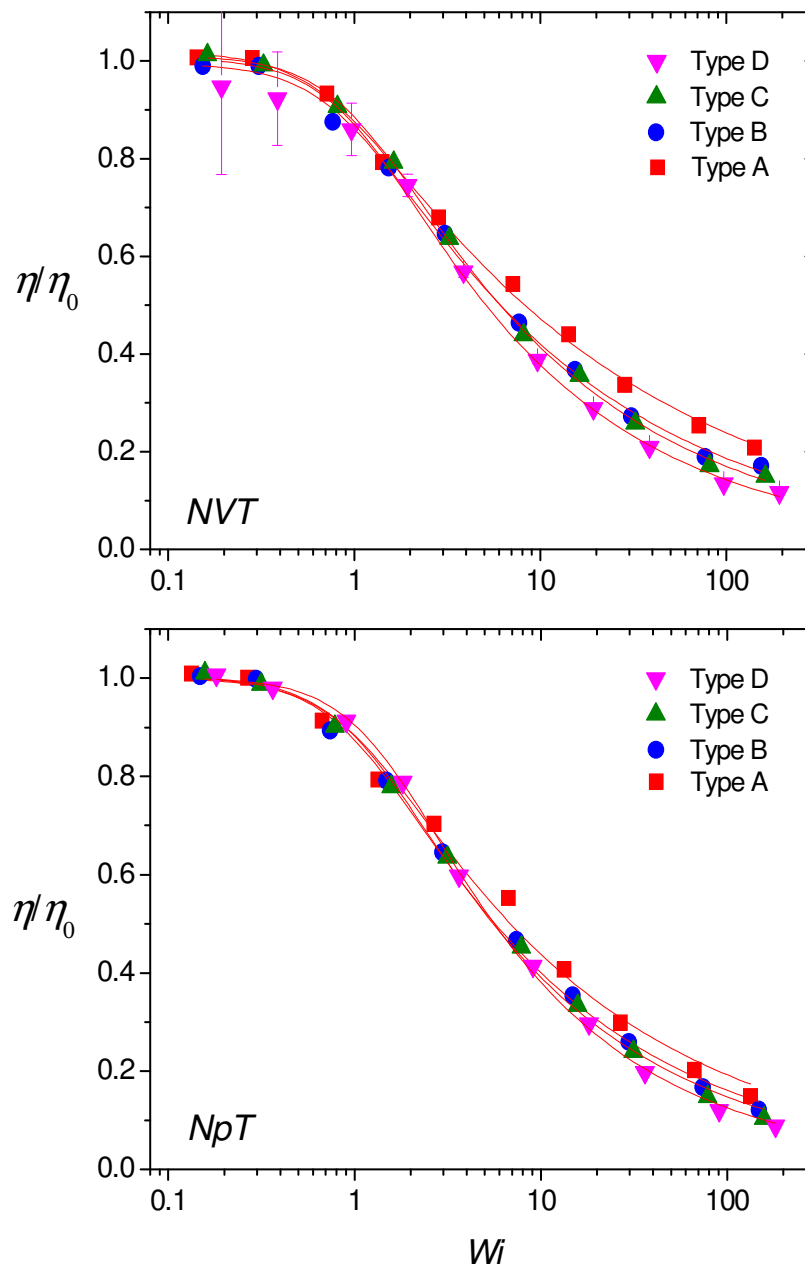


**Figure 6.8.** Shear viscosities versus Weissenberg number calculated from the time constant of the Carreau-Yasuda model for 187 bead hyperbranched polymers with different numbers of spacers in *NVT* and *NpT* simulations (solid lines representing fitting with the Carreau-Yasuda model).

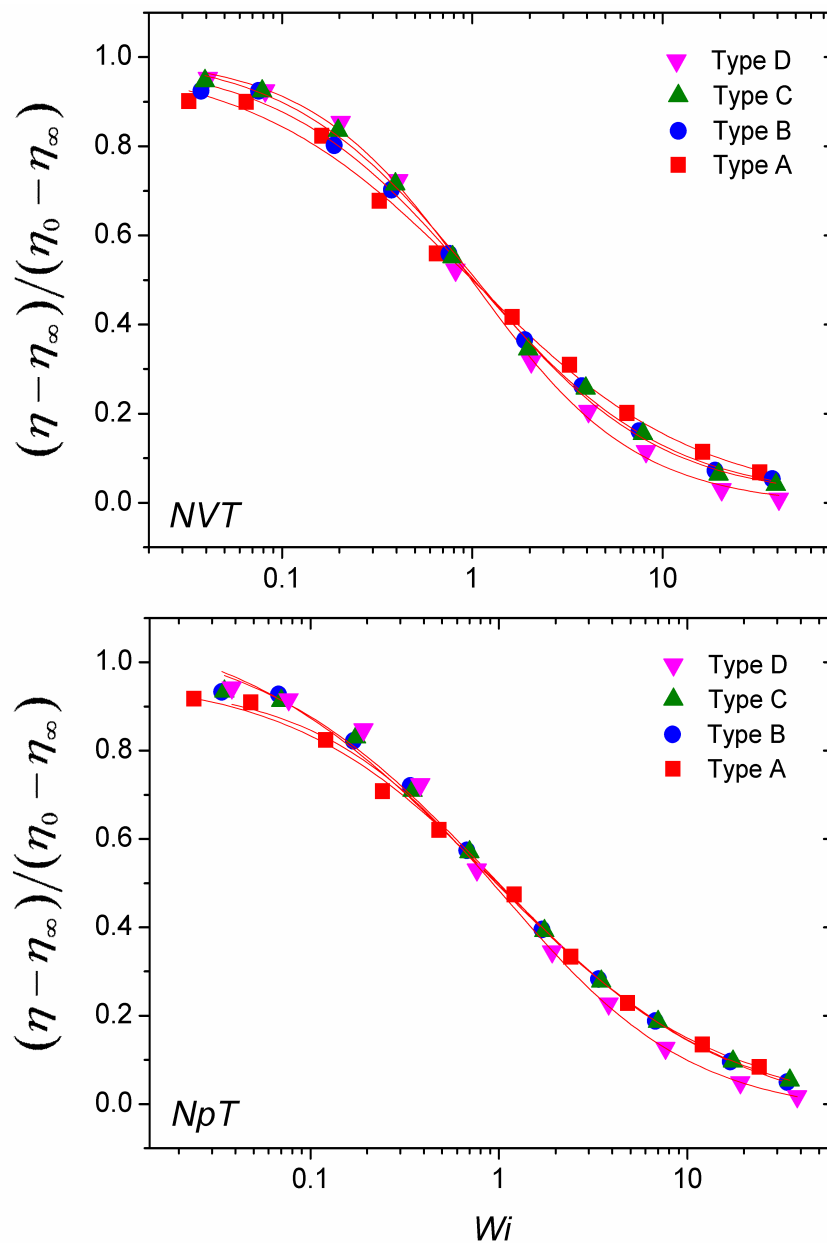


Figure 6.9. Shear viscosities versus Weissenberg number calculated from the time constant of the Cross model for 187 bead hyperbranched polymers with different numbers of spacers in *NVT* and *NpT* simulations (solid lines representing fitting with the Cross model).

### 6.2.3. Shear viscosity of hyperbranched polymer blends

Figure 6.10 presents the shear viscosity of blends of hyperbranched and linear polymers of the same molecular weight at different strain rates in  $NpT$  simulations. Due to statistical uncertainty in the low strain rate region, only results at strain rates from 0.001 are shown. It can be seen that for both type A and D hyperbranched polymers, at lower strain rates, the blend viscosities decrease with increasing proportion of hyperbranched polymers. This suggests fewer entanglements in the system occurred due to the presence of hyperbranched polymers. These findings are in good agreement with previous simulation and experimental results for dendritic polymers (Bosko, 2005, Nunez et al., 2000, Uppuluri et al., 1998). On the other hand, as can be seen from Figure 6.10(c), in the lower strain rate region, the introduction of type A hyperbranched polymer with short branches leads to lower shear viscosity than that for type D polymer with long branches between branching units. This might be due to the larger number of end groups together with a more compact structure, globular molecular shape and lower interpenetration function of type A polymer. However, at higher strain rates, an opposite trend is observed, higher proportion of hyperbranched polymers in the blend results in higher viscosities. This is simply a mixing effect in the blends of hyperbranched polymers and linear chains. At low strain rates, the viscosities of hyperbranched polymers are lower than those of linear chains with equivalent molecular weight whereas at high strain rates, linear chains possess lower viscosities due to stronger chain alignment with the flow. Other authors (Daivis et al., 1992) also observed the same trends where a faster rate of shear thinning for linear molecules leads to a lower viscosity for the linear melt in the high strain rate region. Therefore a combination of hyperbranched polymers and linear analogues has higher shear viscosities than pure hyperbranched polymers and lower viscosities than pure linear chains in the low strain rate region, and vice versa at high strain rates. This can be clearly seen in Figure 6.11 which shows the comparison of the shear viscosity results for the blend of 20% type A polymer with pure hyperbranched and linear polymer melts of equivalent molecular weight of 187 beads per molecule. The value of the blend viscosity always falls in the range between those for hyperbranched and linear chains. The drop of blend viscosities in the Newtonian regime can be attributed to the globular shape of hyperbranched molecules.

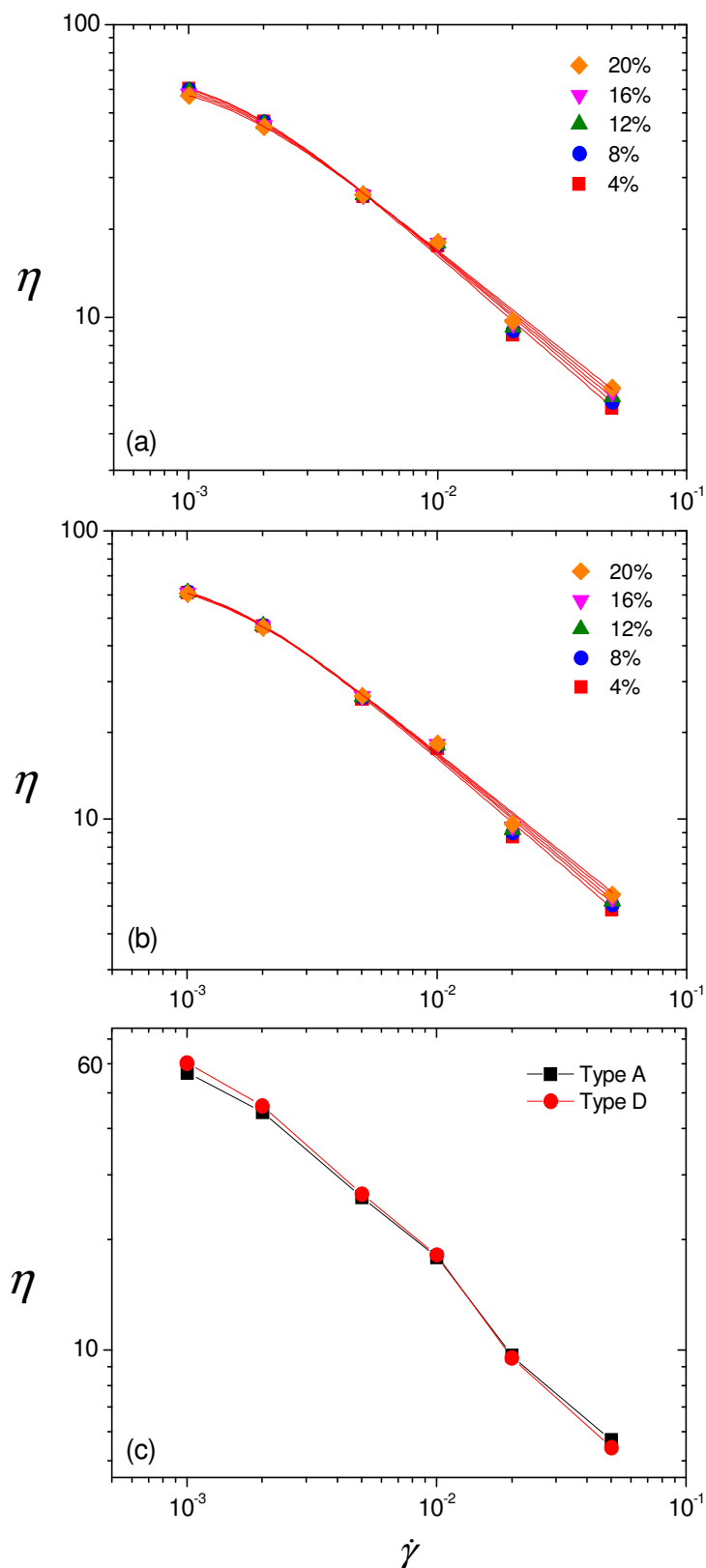
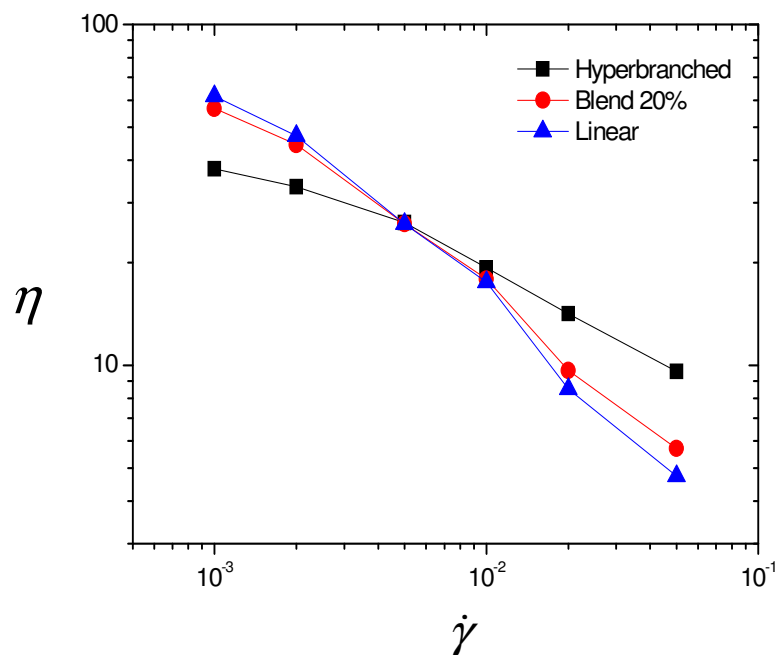


Figure 6.10. Shear viscosity of blends of hyperbranched and linear polymers composed of 187 beads per molecule at different strain rates. (a) Hyperbranched polymer of type A with different blend proportions. (b) Hyperbranched polymer of type D with different blend proportions (solid lines representing fitting with the Carreau – Yasuda equation). (c) Hyperbranched polymers of type A and D with the blend proportion of 20%.



**Figure 6.11.** Comparison of shear viscosity for pure 187 bead hyperbranched polymer of type A, pure 187 bead linear chain and the blend of these polymers with the hyperbranched polymer fraction of 20%.

Shear viscosity data in Figure 6.11 were fitted using the Carreau – Yasuda equation and fitting parameters for blends comprising type A and type D hyperbranched polymers are presented in Tables 6.5 and 6.6 respectively. These data were also fitted using the Cross equation and fitting parameters are shown in Table 6.7 and 6.8. As computed viscosities in the low strain rate region were not considered, the zero shear rate viscosities predicted using the Carreau – Yasuda and the Cross models are quite different. However both of these models suggest that the zero shear rate viscosity value decreases with increasing hyperbranched polymer fraction in the blends. Furthermore the longest relaxation time obtained from the Carreau – Yasuda fit for blends comprising more hyperbranched polymers is higher than that for blends composed of less hyperbranched polymers. In other words, the critical strain rate, at which the transition from Newtonian to non-Newtonian regime occurs, is lower for blends with smaller proportion of hyperbranched polymers. This is in accordance with lower critical strain rate of linear chains compared to hyperbranched polymers of the same molecular weight.

**Table 6.5. Carreau – Yasuda fitting parameters for shear viscosity data of blends of the type A hyperbranched polymers and linear chains of equivalent molecular weight of 187 beads.**

Hyperbranched polymers fraction	$\eta_0$	$\lambda_\eta$	$P_\eta$
4%	71(3)	723(109)	0.37(2)
8%	70(3)	727(107)	0.36(2)
12%	68(3)	730(105)	0.36(2)
16%	67(3)	733(101)	0.35(2)
20%	66(2)	735(99)	0.34(2)

**Table 6.6. Carreau – Yasuda fitting parameters for shear viscosity data of blends of the type D hyperbranched polymers and linear chains of equivalent molecular weight of 187 beads.**

Hyperbranched polymers fraction	$\eta_0$	$\lambda_\eta$	$P_\eta$
4%	74(3)	731(112)	0.37(2)
8%	73(3)	744(112)	0.37(2)
12%	72(2)	758(113)	0.36(2)
16%	71(3)	772(114)	0.35(2)
20%	71(3)	786(114)	0.35(2)

**Table 6.7. Cross fitting parameters for shear viscosity data of blends of type A hyperbranched polymers and linear chains of equivalent molecular weight of 187 beads.**

Hyperbranched polymers fraction	$\eta_\infty$	$\eta_0$	$K$	$m_c$
4%	2(3)	88(17)	467(174)	1.0(2)
8%	2(3)	86(16)	462(168)	1.0(2)
12%	2(2)	85(15)	456(161)	1.0(2)
16%	2(2)	83(14)	450(154)	1.0(2)
20%	2(2)	81(13)	442(146)	1.0(2)

**Table 6.8. Cross fitting parameters for shear viscosity data of blends of the type D hyperbranched polymers and linear chains of equivalent molecular weight of 187 beads.**

Hyperbranched polymers fraction	$\eta_{\infty}$	$\eta_0$	$K$	$m_c$
4%	1(3)	93(19)	532(224)	1.0(2)
8%	1(3)	92(18)	517(213)	1.0(2)
12%	1(3)	91(18)	504(203)	1.0(2)
16%	1(3)	91(18)	493(195)	1.0(2)
20%	1(3)	90(18)	482(187)	1.0(2)

The results show that adding hyperbranched polymers in the melts of linear chains of the same molecular weight does not significantly reduce the viscosity of the system. The shear viscosities of blends drop slightly with increasing proportion of hyperbranched polymers. The reason is that hyperbranched and linear polymers composing the blends have equivalent molecular weight of 187 beads of the same type. In experiments where the presence of a small amount of hyperbranched molecules leads to a substantial drop of viscosities, the molecular weight of linear chains is typically much higher than that of hyperbranched polymers (10 to 40 times higher) (Nunez et al., 2000, Mulkern and Tan, 2000, Hong et al., 1999). On the other hand, our results shows that the viscosity decreases proportionately with the increase of hyperbranched polymer fraction in the blend, whereas some experimental studies found that the viscosity is stabilized after the critical concentration of hyperbranched polymers is reached. In those studies, this limit is caused by the cross-linking and molecular weight buildup due to compatibilization reaction occurring in the blends (Fowler and Baker, 1988, Mulkern and Tan, 2000). The blends in these cases are called reactive blends. In this work, hyperbranched and linear polymers do not have chemical interactions, hence the blends are unreactive and hyperbranched polymers only act as a lubricant. Therefore the viscosities only drop in proportion to the amount of hyperbranched polymers in the blends. This is in agreement with experimental results on hyperbranched polyols and linear styrene maleic anhydride resins (Mulkern and Tan, 2000).

In order to establish a relationship between shear viscosity and blend proportion, viscosities of different blends at different strain rates were plotted against the

hyperbranched polymer fraction in the blends, as presented in Figure 6.12. A linear function,  $\eta = a + c \times H\%$ , was used to fit the data and fitting parameters  $a$  and  $c$  are shown in Tables 6.9 and 6.10. Using these parameters, the blend viscosity at the strain rates considered can be predicted if the value of hyperbranched polymer fraction between 0% (pure linear polymers) to 100% (pure hyperbranched polymers) is given.

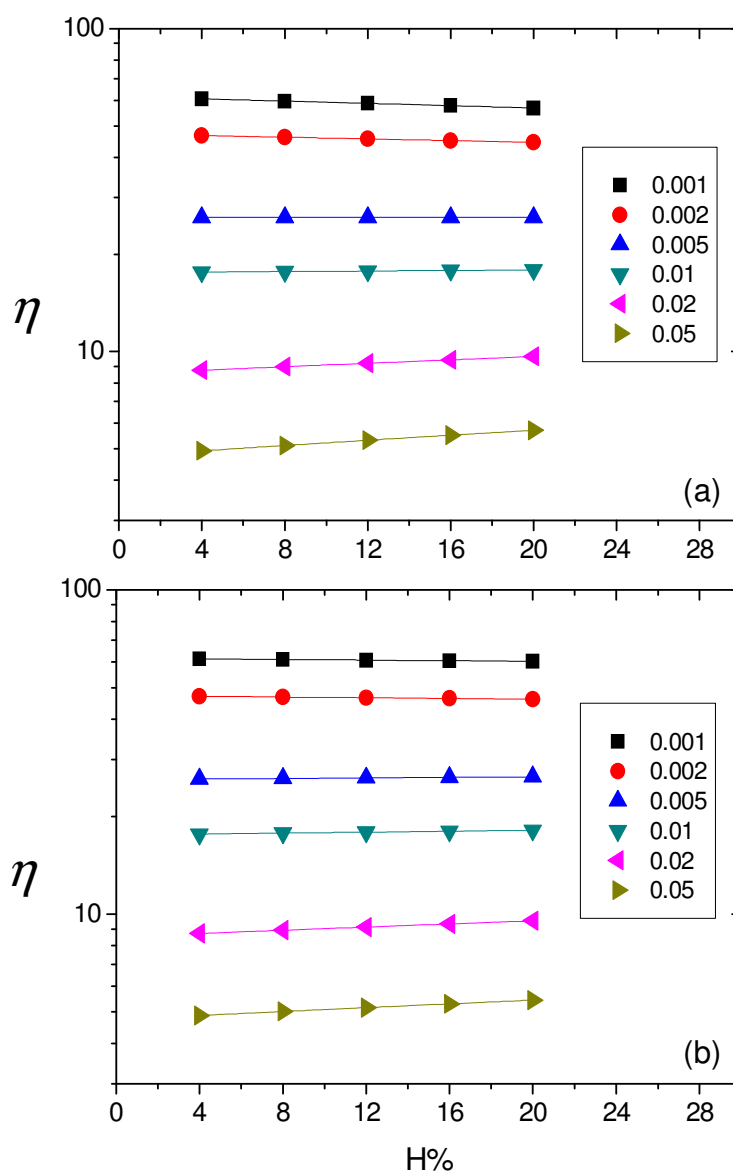


**Figure 6.12. Shear viscosity versus hyperbranched polymer fractions for blends of (a) type A and (b) type D hyperbranched polymers and linear chains of equivalent molecular weight of 187 beads at different strain rates.**

**Table 6.9. Linear fitting parameters for shear viscosity data dependence on hyperbranched polymer fraction for blends comprising type A polymers composed of 187 beads per molecule.**

Strain rate	a	c
0.001	61.59(2)	-0.239(3)
0.002	47.23(3)	-0.138(2)
0.005	26.01(4)	-0.002(1)
0.01	17.55(5)	0.0177(5)
0.02	8.52(3)	0.0567(2)
0.05	4.73(2)	0.0487(3)

**Table 6.10. Linear fitting parameters for shear viscosity data dependence on hyperbranched polymer fraction for blends comprising the type D polymers composed of 187 beads per molecule.**

Strain rate	a	c
0.001	70.04(3)	-0.0683(6)
0.002	47.32(5)	-0.0575(2)
0.005	26.21(1)	0.0268(4)
0.01	17.77(2)	0.030(7)
0.02	8.57(4)	0.0508(3)
0.05	4.75(2)	0.035(1)

### **6.3. First and second normal stress coefficients**

The first and second normal stress coefficients can be defined as  $\psi_1 = (\langle P_{yy} \rangle - \langle P_{xx} \rangle) / \dot{\gamma}^2$  and  $\psi_2 = (\langle P_{zz} \rangle - \langle P_{yy} \rangle) / \dot{\gamma}^2$ , as presented in the first section of this Chapter. These values describe the effect of the normal stress differences exhibited by polymeric fluids. Unlike Newtonian fluids which have the normal stress differences exactly zero in shearing flow, polymeric fluids always have positive first normal stress coefficient which is

usually much larger than the magnitude of the negative second normal stress coefficient (Bird et al., 1987). An increase of these stress coefficients reflects a tendency of the fluid to deform in the normal directions under shear.

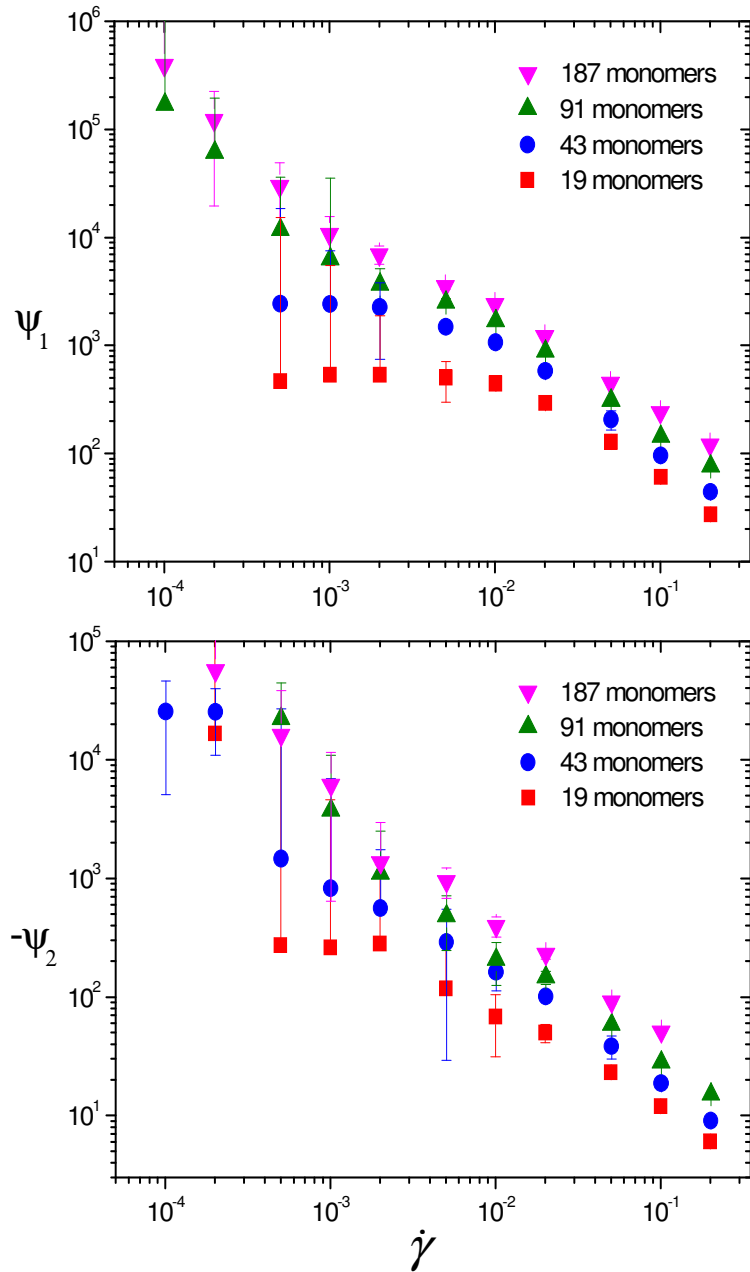
**6.3.1. Normal stress coefficients for hyperbranched polymers of different molecular weights**

Figure 6.13 shows the first and second normal stress coefficients for type A hyperbranched polymers of different molecular weights. For all polymer systems studied, the normal stress coefficients have a large power-law region in which it might decrease by as much as a factor of  $10^6$  for a large molecular system. Furthermore, the rate of decline of the first and second normal stress coefficients with the strain rate is much greater than that of the shear viscosity. In the low shear rate region, the normal stress coefficients reach a plateau as the ratios of  $P_{yy} - P_{xx}$  and  $P_{zz} - P_{yy}$  are proportional to  $\dot{\gamma}^2$  whereas at higher shear rates, the values of the normal stress coefficients rapidly decrease. This again indicates that the hyperbranched polymer fluid has a crossover from Newtonian to non-Newtonian behaviour. At the same strain rate, larger hyperbranched polymers have higher first and second normal stress coefficients as they tend to deform more in comparison with the small molecules. The second normal stress coefficient, which has been studied less extensively in experiments than the first coefficient, is negative and much smaller in magnitude than the first normal stress coefficient. In comparison with other simulation results (Bosko et al., 2004b), our normal stress coefficient values for hyperbranched polymers are larger than those for dendrimers but smaller than those for linear polymers.

Data for the first normal stress coefficient for hyperbranched polymers consisting of 19 and 43 beads were fitted using the Carreau-Yasuda model. The zero shear rate first normal stress coefficients  $\psi_{1,0}$  for these systems were found to be 508(13) and 2430(45) respectively. From these values and zero shear rate viscosities  $\eta_0$  obtained from the Carreau-Yasuda fit for shear viscosity, the viscous relaxation time  $\tau_v$  can be computed.

The viscous relaxation time, which is defined by  $\tau_v = \int_0^\infty tG(t)dt / \int_0^\infty G(t)dt$  where  $G(t)$  is the stress relaxation modulus from the theory of linear viscoelasticity (Ferry, 1980), can be calculated by the expression  $\tau_v = \psi_{1,0} / 2\eta_0$ . For hyperbranched polymers

comprising 19 and 43 beads, the values of  $\tau_v$  were found to be 25(3) and 67(7) respectively. These values are in very good agreement with the time constants  $K$  obtained from the Cross model which were found to be 24(9) and 60(10) for those hyperbranched polymer systems.



**Figure 6.13. First and second normal stress coefficients versus strain rate for type A hyperbranched polymers of different molecular weights.**

The normal stress coefficients for all hyperbranched polymers were fitted in the power-law region and the values of the exponents of the asymptotic dependences  $\psi_1 \propto \dot{\gamma}^{-\alpha}$  and

$|\psi_2| \propto \dot{\gamma}^{-\beta}$  are presented in Table 6.11. The values of these exponents are within the range of experimental values for polymer melts and concentrated solutions (Bird et al., 1987). Similar to NEMD simulation results for dendrimer melts (Bosko, 2005), the values of the  $\alpha$  and  $\beta$  exponents do not vary systematically with the size of the hyperbranched polymer molecules. This is in contrast with results for linear polymers (Bosko, 2005) which have the values of  $\alpha$  and  $\beta$  increasing with the chain lengths.

**Table 6.11. Estimated values of the exponents in the power-law regions for the first and second normal stress coefficients of type A hyperbranched polymers.**

Number of beads	$\alpha$	$\beta$
19	1.09(4)	0.96(2)
43	1.09(2)	1.0476(9)
91	1.05(3)	0.96(2)
187	1.00(2)	0.91(3)

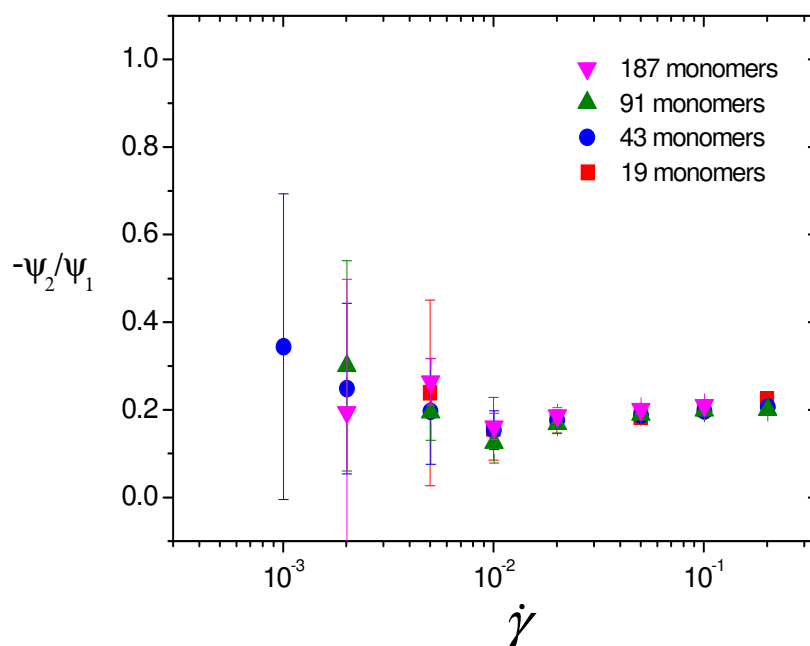


**Figure 6.14. Ratio of the second and first normal stress coefficients for type A hyperbranched polymers of different molecular weights.**

The ratios of  $-\psi_2/\psi_1$  are presented in Figure 6.14 which shows that the values of  $-\psi_2/\psi_1$  are approximately 0.2 for type A all hyperbranched polymer systems. This is very similar to simulation results for dendrimers as they all have compact, highly

branched architectures with globular shape and internal bond constraints which prevent pronounced stretching of the molecules.

### 6.3.2. Normal stress coefficients of hyperbranched polymers with different numbers of spacers

Values of  $\psi_1$  and  $-\psi_2$  for 187 bead hyperbranched polymers with different numbers of spacers obtained from *NVT* and *NpT* simulations are shown in Figures 6.15 and 6.16. It can be seen that the first and second normal stress coefficients are always higher for systems with longer branches. However, the gap between the values of the normal stress coefficients of different hyperbranched polymers is more pronounced for  $\psi_1$  than that for  $-\psi_2$ . The crossover from Newtonian to non-Newtonian behaviour cannot be captured due to the ‘noise’ of data in the low strain rate region. The normal stress coefficients for all simulated hyperbranched polymers in *NpT* and *NVT* simulations were fitted in the power-law region.

The exponents  $\alpha$  and  $\beta$  of the asymptotic dependences  $\psi_1 \propto \dot{\gamma}^{-\alpha}$  and  $|\psi_2| \propto \dot{\gamma}^{-\beta}$  are presented in Table 6.12. Similar to the behaviour of the shear viscosity, the decreasing rate of the normal stress coefficients is more pronounced for *NpT* simulations, hence the exponents  $\alpha$  and  $\beta$  obtained from *NpT* simulations have higher values than those from *NVT* simulations. However, these values are still within the range of experimental values for polymer melts and concentrated solutions (Bird et al., 1987).

**Table 6.12. Estimated values of the exponents in the power law regions for the first and second normal stress coefficients of 187 bead hyperbranched polymers with different numbers of spacers.**

Type of hyperbranched polymers	<i>NVT</i>		<i>NpT</i>	
	$\alpha$	$\beta$	$\alpha$	$\beta$
Type A	1.0(2)	0.9(7)	1.2(5)	1.27(4)
Type B	1.1(1)	1.0(3)	1.2(6)	1.26(9)
Type C	1.0(9)	1.1(1)	1.1(9)	1.1(3)
Type D	1.1(5)	1.1(4)	1.2(6)	1.1(6)

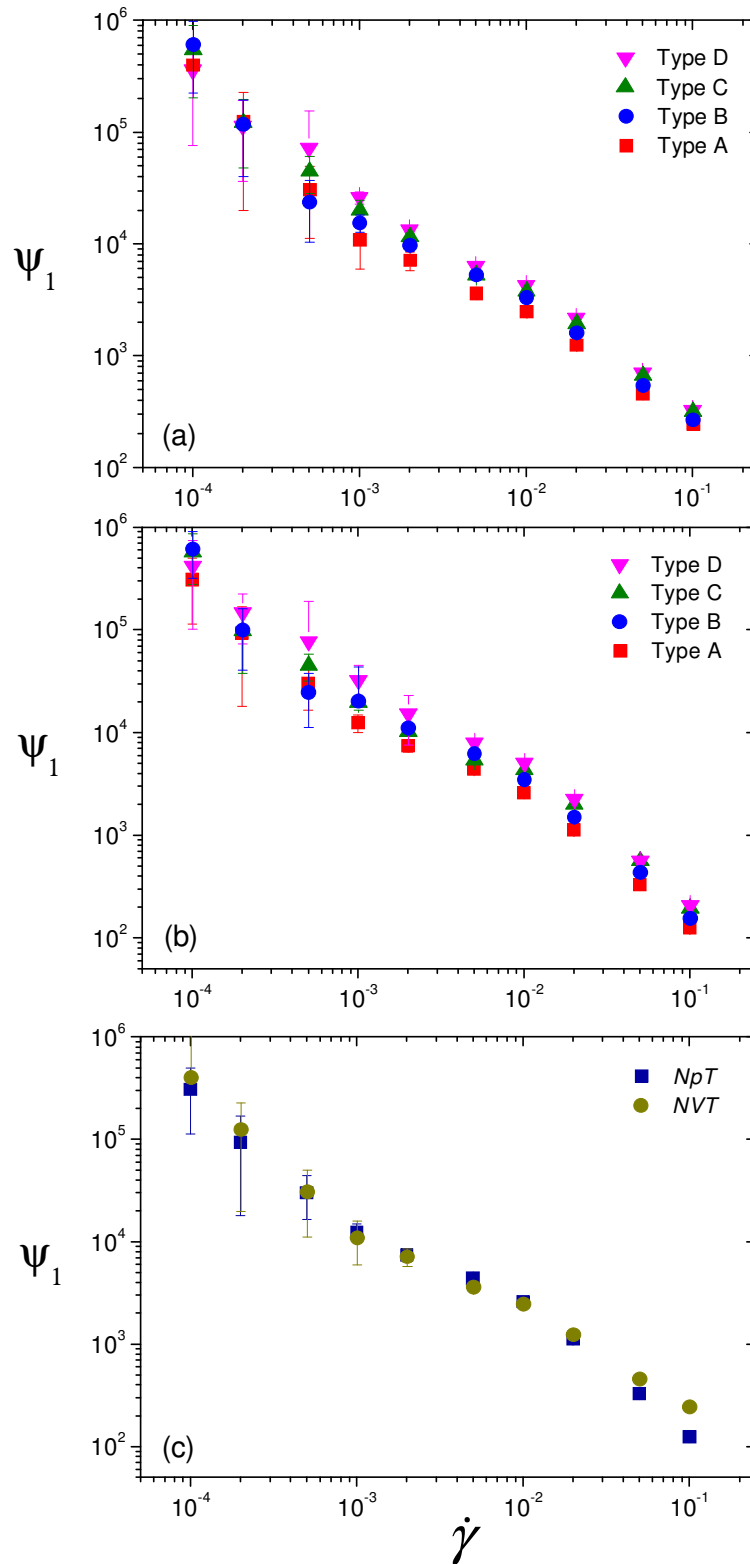


**Figure 6.15.** First normal stress coefficient versus strain rate for 187 bead hyperbranched polymers (a) with different numbers of spacers in *NVT* simulations, (b) with different numbers of spacers in *NpT* simulation and (c) of type A in *NVT* and *NpT* simulations.

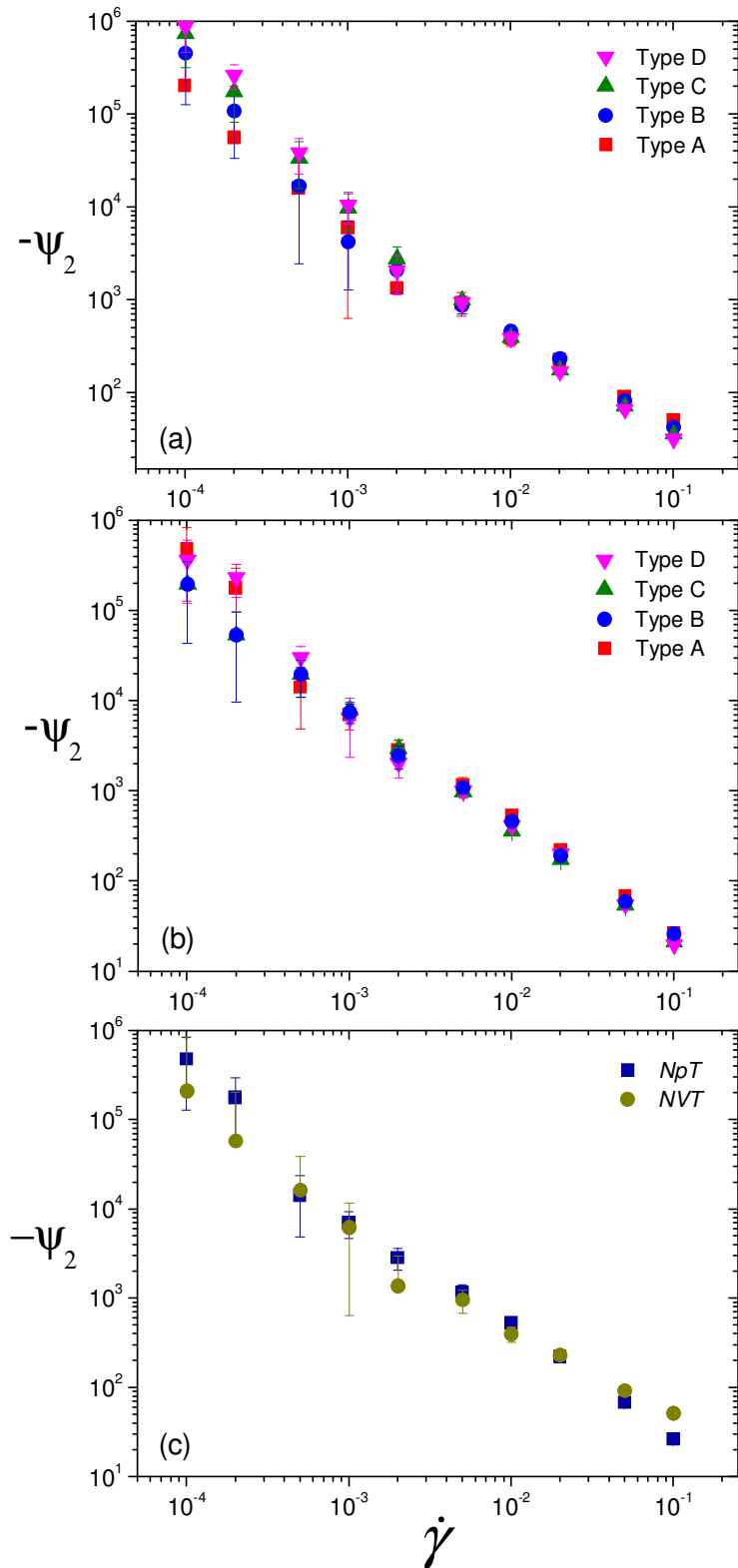


**Figure 6.16.** Second normal stress coefficient versus strain rate for 187 bead hyperbranched polymers (a) with different numbers of spacers in NVT simulations, (b) with different numbers of spacers in NpT simulation and (c) of type A in NVT and NpT simulations.

### ***6.3.3. Normal stress coefficients of hyperbranched polymer blends***

Figure 6.17 shows the first normal stress coefficients for blends of hyperbranched polymers and linear chains of the same molecular weight of 187 beads at different strain rates. As can be seen, there is no significant difference in the value of the normal stress coefficients between blends with different proportion of hyperbranched polymers. However it can still be observed that the pressure difference (between the  $x$  and  $y$  diagonal elements of the pressure tensor) is slightly stronger for blends with smaller hyperbranched polymer fraction at most of the considered strain rates. However, the difference between the first normal stress coefficients is typically about 5% for blends when the hyperbranched polymer ratios differ by 4%, as shown in the inset graph of Figure 6.17. This is similar to the behaviour of blends of dendrimers and linear polymers in NEMD simulations at constant pressure (Bosko, 2005).

Figure 6.18 presents the second normal stress coefficients for these simulated blends comprising hyperbranched polymers and linear analogues in the low strain rate region. Similar to the first normal stress coefficients, the pressure difference (between the  $y$  and  $z$  diagonal elements of the pressure tensor) does not change significantly with increasing proportion of hyperbranched polymers in the blends.

In comparison with pure hyperbranched polymers and pure linear analogues, the normal stress coefficient results for the blends of these polymers are always in between, as shown in Figure 6.19. However, the stress coefficients of the blends are closer to those of pure linear systems than to those of pure hyperbranched polymers because the proportion of hyperbranched polymers in the blends is small.

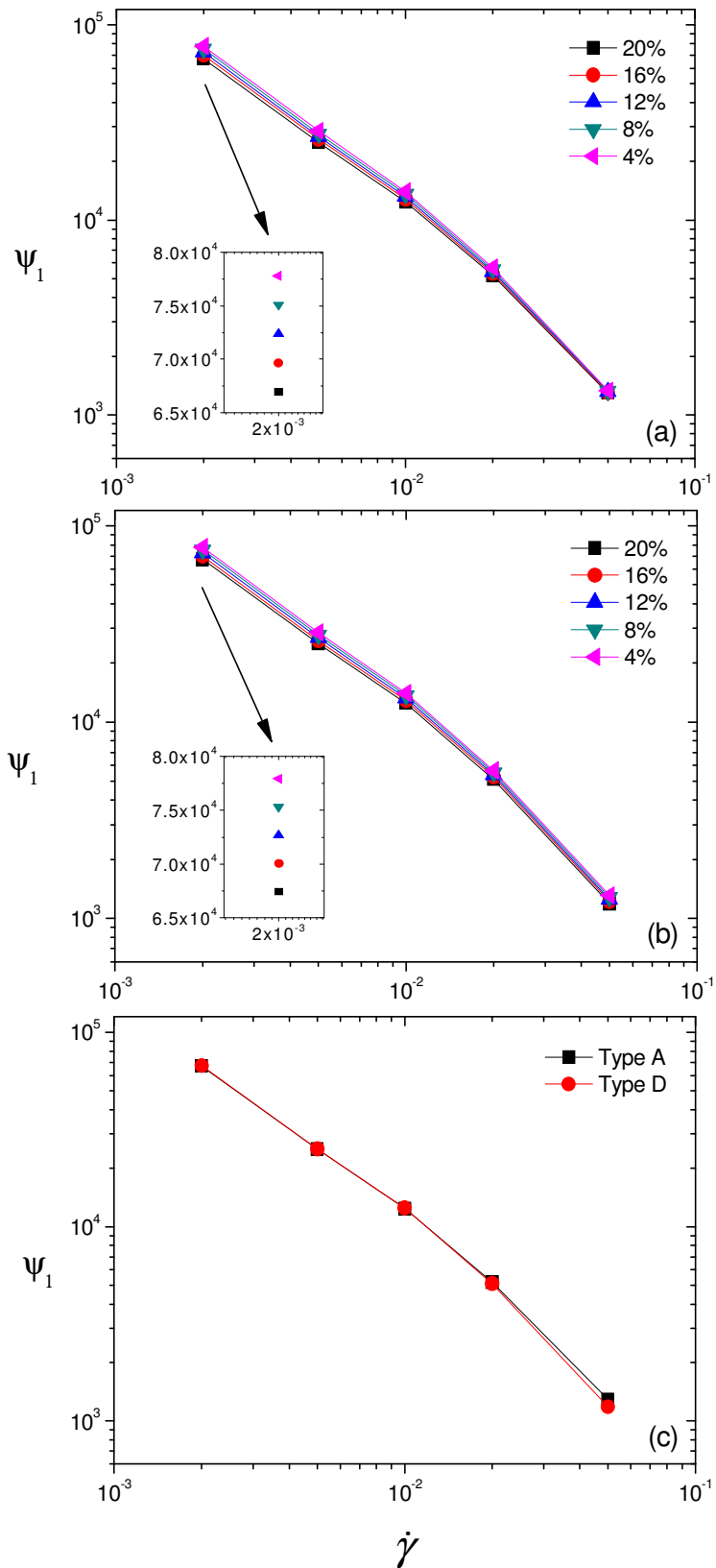


**Figure 6.17.** First normal stress coefficients of blends of hyperbranched and linear polymers composed of 187 beads per molecule at different strain rates.  
 (a) Hyperbranched polymer of type A with different blend proportions.  
 (b) Hyperbranched polymer of type D with different blend proportions.  
 (c) Hyperbranched polymers of type A and D with the blend proportion of 20%.

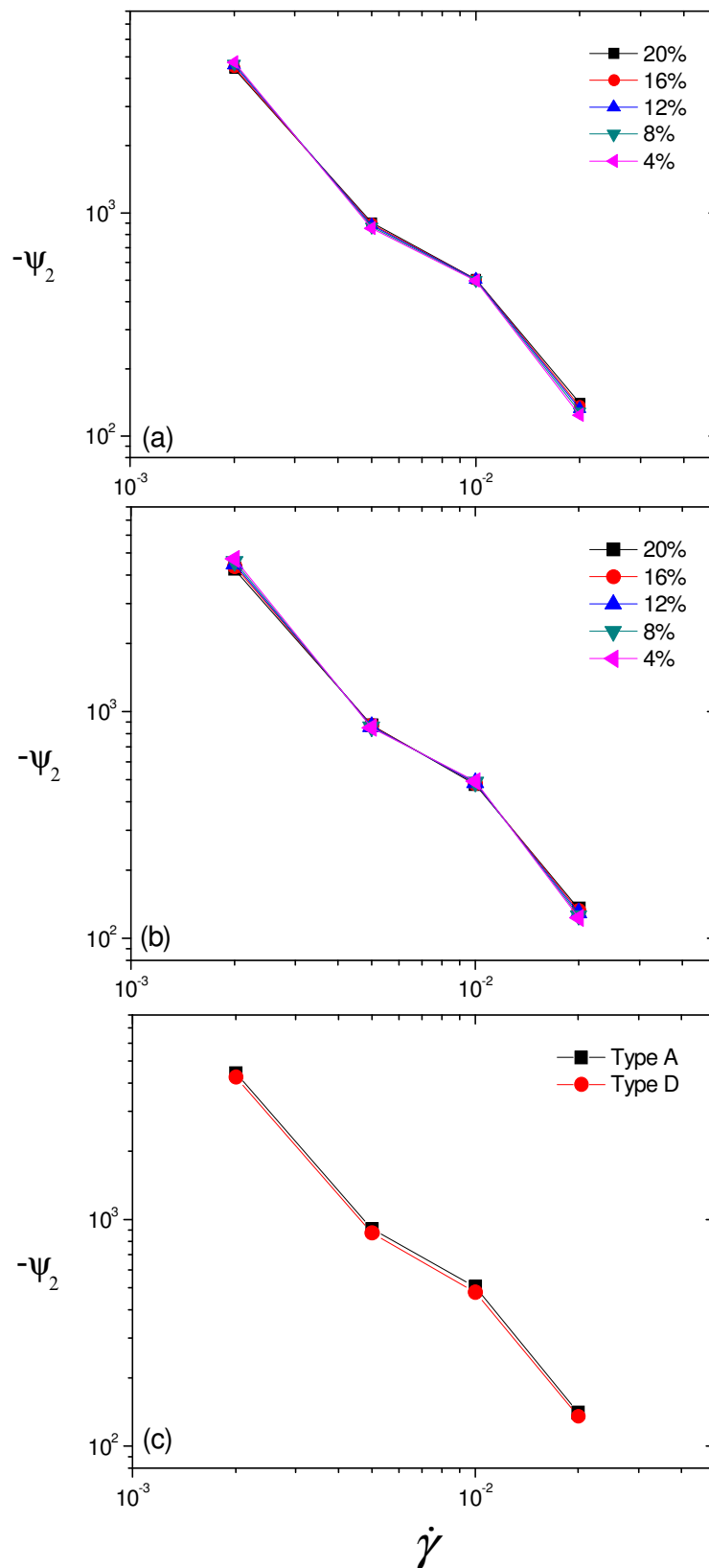
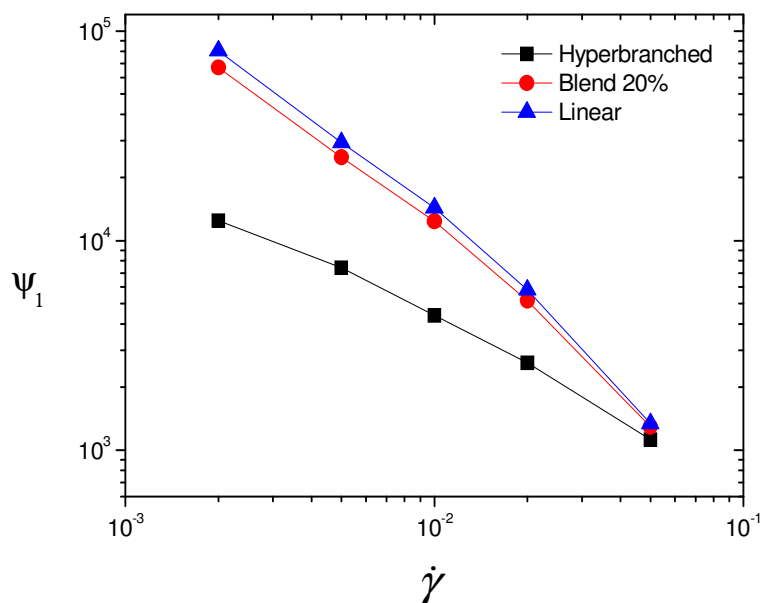


Figure 6.18. Second normal stress coefficients of blends of hyperbranched and linear polymers composed of 187 beads per molecule at different strain rates.  
(a) Hyperbranched polymer of type A with different blend proportions.  
(b) Hyperbranched polymer of type D with different blend proportions.  
(c) Hyperbranched polymers of type A and D with the blend proportion of 20%.



**Figure 6.19.** Comparison of first normal stress coefficients for pure hyperbranched polymer of type A, pure linear chain and the blend of these polymers with the hyperbranched polymer fraction of 20% (all these polymers have the same molecular weight of 187 beads).

## 6.4. Pressure and density

### 6.4.1. Pressure of hyperbranched polymers of different molecular weights

Figure 6.20 shows the isotropic pressure of the sheared hyperbranched polymer systems of type A in *NVT* simulations, which can be calculated as:

$$p = \frac{1}{3} \text{Tr}(\mathbf{P}) = \frac{1}{3} (\langle P_{xx} \rangle + \langle P_{yy} \rangle + \langle P_{zz} \rangle) \quad (6.9)$$

At low strain rates, the pressure of low molecular weight hyperbranched polymer fluids is higher than that of high molecular weight polymer fluids while at high strain rates, the pressure of the high molecular weight fluids increases earlier and more rapidly than that of the low molecular weight ones. This can be explained by the behaviour of different molecules under shear, as presented in the previous Chapter, namely that molecules of high molecular weight hyperbranched polymers become aspherical more quickly under shear than for low molecular weight polymers.

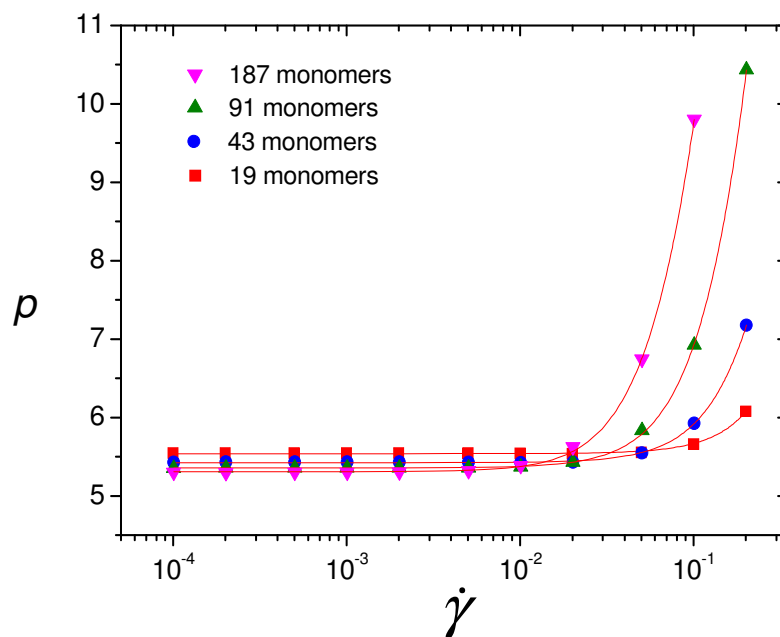


**Figure 6.20.** Dependence of the isotropic pressure on strain rate for type A hyperbranched polymers of different molecular weights (solid lines representing fitting with the Carreau-Yasuda model).

Fitting the pressure data using the Carreau-Yasuda model  $p = p_0 / \left[ 1 + (\lambda_p \dot{\gamma})^2 \right]^{m_p}$  which has been applied for shear viscosity data, the zero shear pressure of hyperbranched polymers can be investigated. The values of the zero shear pressure  $p_0$  are 5.540(3), 5.414(3), 5.349(6) and 5.299(8) for hyperbranched polymers composed of 19, 43, 91 and 187 monomers respectively. The critical strain rate at which the transition from Newtonian to non-Newtonian behaviour of the pressure occurs can be evaluated as the inverse of  $\lambda_p$  obtained from the Carreau-Yasuda model. The critical strain rate was found to have the value of 0.217(2), 0.126(5) and 0.06(2) for hyperbranched polymers comprising 43, 91 and 187 monomers respectively. For hyperbranched molecules composed of 19 monomers, the value of  $\lambda_p$  obtained is very small and the value of the standard error is large, hence the critical strain rate calculated is uncertain. In comparison to the critical strain rate for viscosity, the value of  $\dot{\gamma}_c$  for pressure is higher because a higher shear rate is required to distort the radial distribution function than that to distort the whole molecule. The trend of pressure changes due to strain rate observed here for hyperbranched polymer melts is similar to that seen previously in dendrimer melts and falls within the range between dendrimer and linear polymer melts (Bosko et al., 2004b). This is because dendrimers

have the most compact architecture, whereas hyperbranched polymers are less compact and linear polymers have the largest spatial separation of monomers. This behaviour can be found not only for dendritic polymer melts but also for solutions. It has been reported by Lue (Lue, 2000) that dendritic polymers in low concentration solution have lower pressure than linear polymers in *NVT* simulations. In addition, it was found that concentrated solutions of low-generation dendrimers show similar behaviour to linear polymers and the pressure increases more rapidly with concentration for high-generation dendrimers.

**6.4.2. Pressure and density of hyperbranched polymers with different numbers of spacers**

Results of the isotropic pressure for hyperbranched polymers with the same molecular weight of 187 beads per molecule but different numbers of spacers in *NVT* simulations are shown in Figure 6.21(a). It can be seen that at low strain rates, the pressure of all systems is roughly constant while at high strain rates, the pressure increases rapidly. This indicates that the behaviour of the isotropic pressure moves from the Newtonian to non-Newtonian regime. In comparison to linear and other branched polymers, the pressure for hyperbranched polymers shows a different trend due to the effect of the shape and branching. It has been reported by several authors (Jabbarzadeh et al., 2003, Kim et al., 2008) that before increasing rapidly, a drop can be observed in the plot of  $p$  versus  $\dot{\gamma}$  for linear, star, H or comb-shaped polymer melts. We do not observe this behaviour for hyperbranched polymers simulated to the same degree, the pressure only slightly drops. The pressure data were fitted using the Carreau-Yasuda equation (Bird et al., 1987)  $p = p_0 / \left[ 1 + (\lambda_p \dot{\gamma})^2 \right]^{m_p}$  where  $p_0$  is the zero shear rate pressure,  $\lambda_p$  is a time constant and  $m_p$  is the power law exponent. Fitting parameters are shown in Table 6.13. As can be seen from this Table, the zero shear rate isotropic pressure increases slightly with increasing number of spacers due to the larger spatial separation of beads. Furthermore, the critical strain rate  $\dot{\gamma}_c$  at which the transition from Newtonian to non-Newtonian behaviour of the pressure occurs can be calculated as the inverse of  $\lambda_p$ . The values of  $\dot{\gamma}_c$  were found to be 0.06(2), 0.07(3), 0.09(2) and 0.09(2) for hyperbranched polymers with the number of spacers of 2, 3, 4 and 5 respectively.

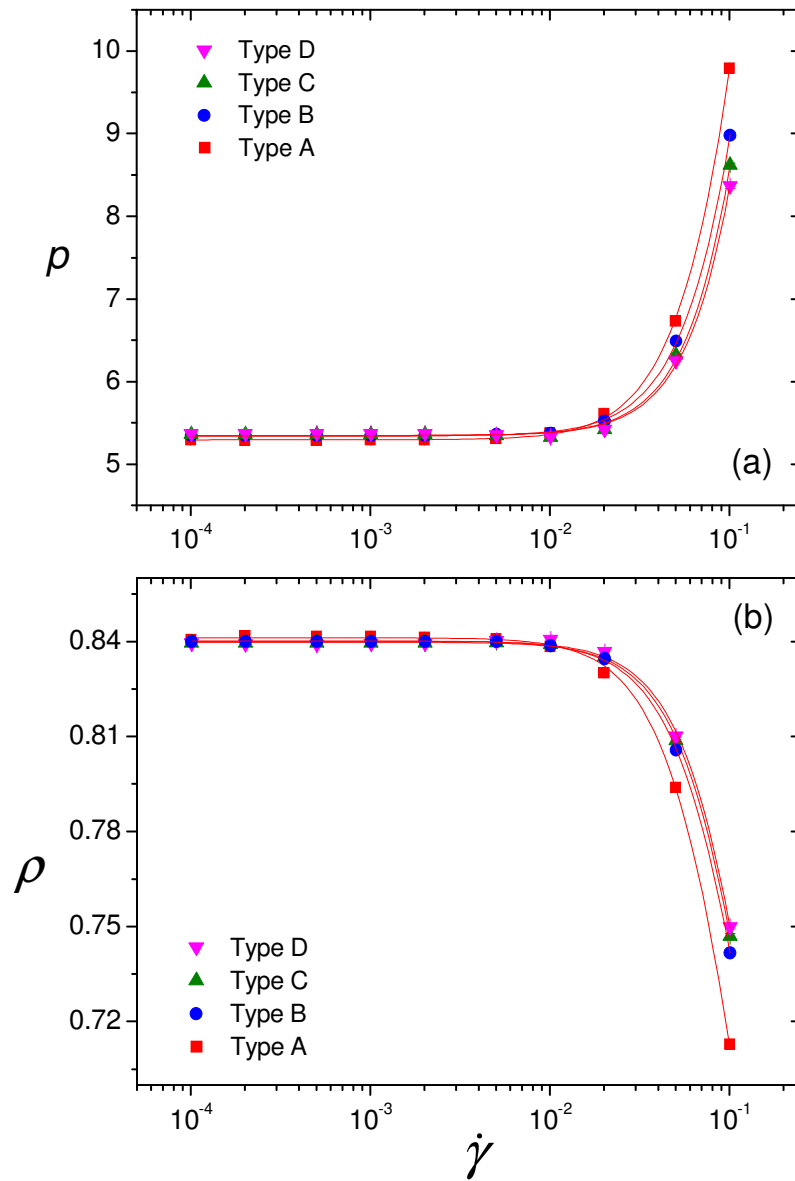


Figure 6.21. Dependence of the (a) isotropic pressure and (b) reduced bead density on strain rate of 187 bead hyperbranched polymers with different numbers of spacers in  $NVT$  and  $NpT$  simulations respectively (solid lines representing fitting with the Carreau-Yasuda model).

**Table 6.13. Parameters of the Carreau-Yasuda model fitted to the isotropic pressure versus strain rate dependence for hyperbranched polymers with the same molecular weight of 187 beads but different numbers of spacers.**

Type of hyperbranched polymers	$p_0$	$\lambda_p$	$m_p$
A	5.295(6)	16.9(7)	-0.46(2)
B	5.334(4)	14.1(7)	-0.48(3)
C	5.336(9)	11(2)	-0.6(1)
D	5.34(1)	11(3)	-0.6(3)

As opposed to  $NVT$  simulations with constant density and changing pressure,  $NpT$  simulations have constant pressure and changing density. Figure 6.21(b) shows the reduced bead density profile in constant pressure simulations. It can be seen that the density remains constant at low strain rates while at high strain rates, the density falls rapidly. This phenomenon is called ‘shear dilatancy’ (Reynolds, 1885). Density data are fitted using Carreau-Yasuda equation  $\rho = \rho_0 / \left[ 1 + (\lambda_p \dot{\gamma})^2 \right]^{m_p}$  where  $\rho_0$  is the zero shear rate density,  $\lambda_p$  is a time constant from and  $m_p$  is the power law exponent. Results of these parameters are presented in Table 6.14. The time constant for density  $\lambda_p$  has lower values than those for isotropic pressure  $\lambda_p$ . Therefore the critical strain rates for the reduced bead density are higher than those for the pressure.

**Table 6.14. Parameters of the Carreau-Yasuda model fitted to the reduced bead density versus strain rate dependence for hyperbranched polymers with the same molecular weight of 187 beads but different numbers of spacers.**

Type of hyperbranched polymers	$\rho_0$	$\lambda_p$	$m_p$
A	0.8412(2)	12.6(5)	0.175(9)
B	0.8400(1)	11.1(3)	0.156(6)
C	0.8400(2)	9.4(8)	0.18(2)
D	0.8400(4)	9(2)	0.21(9)

**6.4.3. Density of blends of hyperbranched and linear polymers**

Densities of blends of linear polymer and different hyperbranched polymers in the melts in  $NpT$  simulations are presented in Figure 6.22. As can be seen, at low strain rates, the densities of all systems simulated remain constant and these values for different blend compositions are very close. The zero shear rate density obtained from fitting the density data using the Carreau-Yasuda equation slightly increases with increasing proportion of hyperbranched polymers in the blends, as seen in Table 6.15. This can be explained by the difference in topologies of entangled, less compact linear chains and unentangled, more compact hyperbranched polymers, which lead to the increase in density when more hyperbranched polymers are added to the melts of linear analogues. In the linear regime with higher strain rates, the slope of the density vs. strain rate curve varies more when the hyperbranched polymer fraction rises. This is consistent with the behaviour of the shear viscosities as well as the normal stress coefficients of these blends. Furthermore the densities for blends composed of type A hyperbranched polymers are slightly higher than those for blends comprising type D polymers due to the shorter branches and more dense structure of type A molecules.

**Table 6.15. Zero shear rate density for blends of 187 bead hyperbranched and 187 bead linear polymers with different hyperbranched polymer fractions.**

Type of hyperbranched polymers	4%	8%	12%	16%	20%
A	0.8370(2)	0.8370(1)	0.8372(1)	0.8373(1)	0.8375(2)
D	0.8364(1)	0.8365(1)	0.8366(2)	0.8370(2)	0.8372(1)

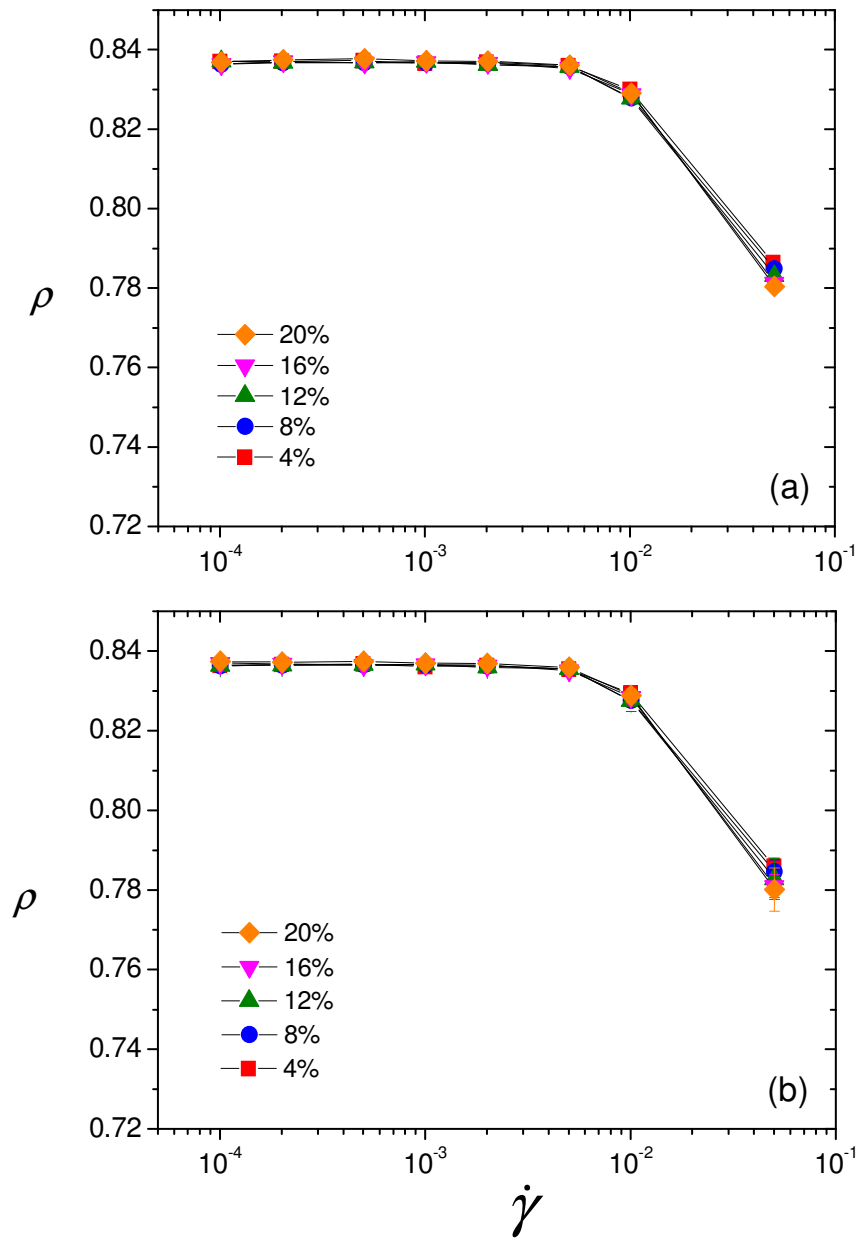


Figure 6.22. Density of blends of 187 bead linear polymers and 187 bead hyperbranched polymers of (a) type A and (b) type D with different hyperbranched polymer proportions.

## 6.5. Stress-optical rule

In order to characterize the relationship between macroscopic stress and the microscopic processes such as rotations and deformations of bonds (Wales, 1976), the stress-optical rule (SOR) can be tested from the bond alignment tensor and stress tensor. It states that the mechanical and optical tensors are coaxial and proportional to each other.

### 6.5.1. Stress-optical rule for hyperbranched polymers of different molecular weights

Figure 6.23 presents the ratio of  $(P_{xx} - P_{yy})$  and  $(S_{xx} - S_{yy})$  as well as that of  $(P_{yy} - P_{zz})$  and  $(S_{yy} - S_{zz})$  for type A hyperbranched polymers of different molecular weight. As can be seen, the components of the stress and alignment tensor are proportional at low strain rates. The proportionality constant, which is called the stress-optical coefficient, is independent of molecular weight. For all hyperbranched polymer systems, this coefficient has the value of approximately 3.3(3). The lack of dependence of the stress-optical coefficient on molecular weight for simulated hyperbranched polymers is in good agreement with experimental results which showed that the stress-optical coefficient is a function of the local condition such as the temperature, solvent or polymer concentration but does not depend on the features of molecular structure on a large length-scale such as molecular weight, molecular weight distribution, branching or degree of cross-linking (Doi and Edwards, 1986). At high strain rates, the SOR is invalid for all simulated hyperbranched polymers. The reason is that the micro structure of hyperbranched polymer melts is not included in the bond order tensor whereas the stress is determined by the alignment, deformation and micro structure of the systems. The SOR does not take into account the flow-induced changes of the radial distribution function which is distorted at high strain rates.

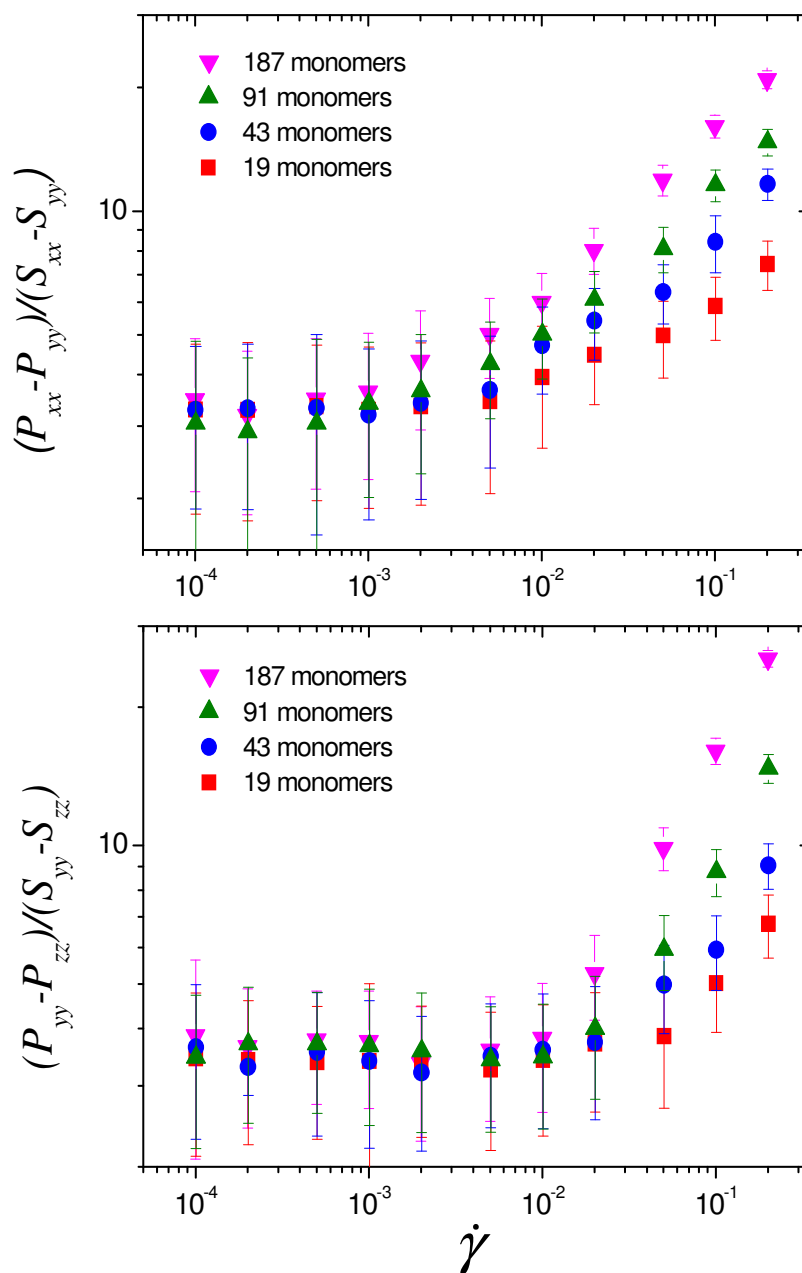


**Figure 6.23.** Deviations from the stress-optical rule  $-(P_{xx} - P_{yy}) / (S_{xx} - S_{yy})$  and  $(P_{yy} - P_{zz}) / (S_{yy} - S_{zz})$  versus  $\dot{\gamma}$  for type A hyperbranched polymers of different molecular weights.

It has been discussed elsewhere that the failure of the SOR could be due to the influence of the molecular weight distribution (van Meerveld, 2004), the chain conformation (Sridhar et al., 2000), or the role of the number of entanglements in the fluid (Rothstein and McKinley, 2002). There are also certain types of systems that do not follow the SOR at all such as rod-like polymers in the concentrated isotropic regime (Mead and Larson, 1990). In experiments, the experimental conditions can also lead to the failure of the SOR, such as performing experiments near the glass transition temperature (Kroger et al., 1997, Wales, 1976) or at a rate higher than the inverse of the Rouse time of the chain in an elongational experiment (Venerus et al., 1999). The SOR fails also because while birefringence saturates, the stress can continue to grow without limit (Wagner, 2006). These factors are not present in our study, hence we can deduce that the SOR is violated as flow-induced changes of the micro structure of hyperbranched polymers were not taken into account at high strain rates.

### ***6.5.2. Stress-optical rule for hyperbranched polymers with different number of spacers***

Figure 6.24 shows the deviations from the SOR for hyperbranched polymers with the same molecular weight of 187 beads but different number of spacers. As can be seen, components of the stress and alignment tensors are proportional, hence the SOR is valid, only in the low strain rate region. The proportionality constant – the stress-optical coefficient – is independent of the number of spacers and has the value of approximately 3.2(3) which is very close to the obtained stress optical coefficient for hyperbranched polymers of type A at different molecular weight. This is in agreement with experimental results which show that the stress optical coefficient does not depend on the molecular weight or branching of molecules (Doi and Edwards, 1986). As discussed in the previous section, the violation of the SOR in the high strain rate region is because it does not take into account the flow-induced changes of the radial distribution function of hyperbranched polymers that is distorted at high strain rates.

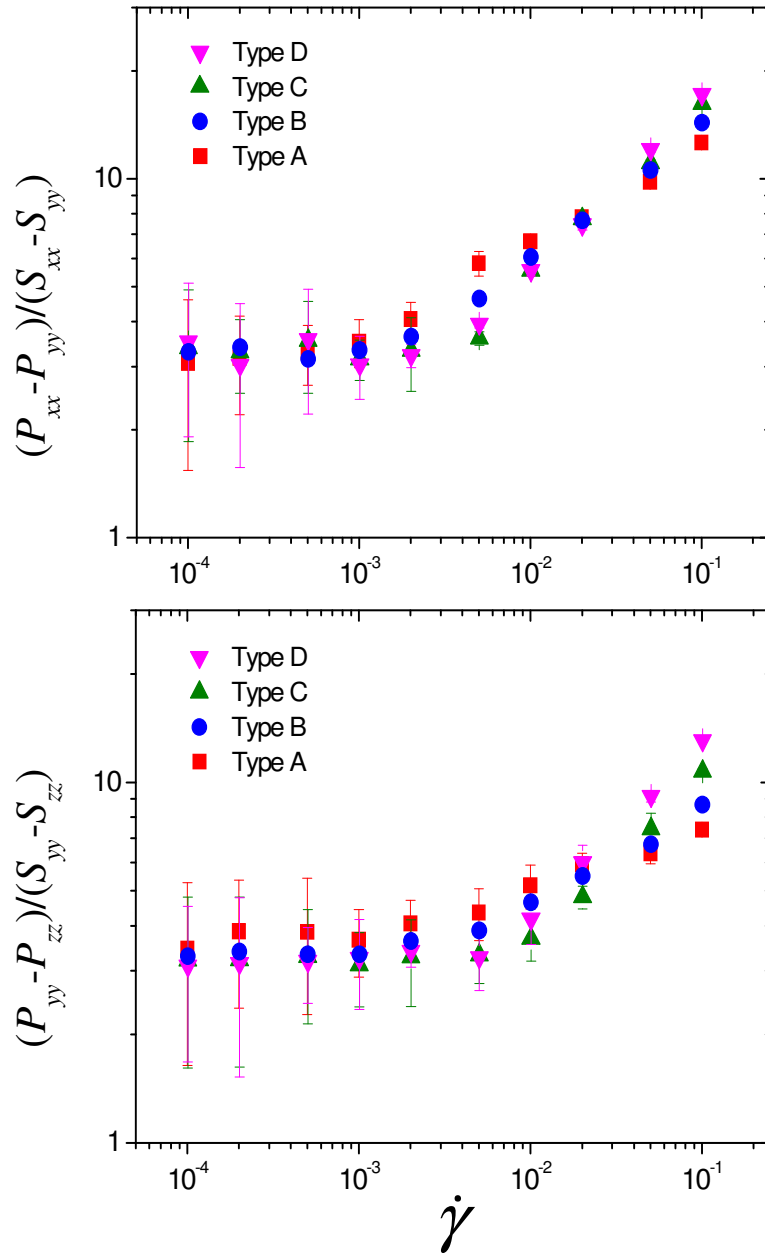


**Figure 6.24.** Deviations from the stress-optical rule –  $(P_{xx} - P_{yy}) / (S_{xx} - S_{yy})$  and  $(P_{yy} - P_{zz}) / (S_{yy} - S_{zz})$  versus  $\dot{\gamma}$  for hyperbranched polymers with the same molecular weight of 187 beads but different numbers of spacers.